A wave-flume study of scour at a pile breakwater: solitary waves

Conghao Xu[a], Zhenhua Huang[a,*], Yu Yao[b]

[a]*Department of Ocean and Resources Engineering, School of Ocean and Earth Science and Technology, University of Hawaii at Manoa, Honolulu HI 96822 USA*
[b]*Changsha University of Science and Technology, Changsha, Hunan, China*

Abstract

Understanding the sediment transport and the resulting scour around coastal structures such as pile breakwaters under local extreme wave conditions is important for the foundation safety of various coastal structures. This study reports a wave-flume experiment investigating the scour induced by solitary waves at a pile breakwater, which consists of a row of closely spaced large piles. A wave blacking gate with a simple operation procedure in the experiment was designed to eliminate possible multiple reflections of the solitary wave inside the flume. An underwater laser scanner and a point probe were used in combination to provide high-resolution data of the bed profile around the pile breakwater. Effects of incident wave height and local water depth on the maximum scour depth, the maximum deposition height and the total scour and deposition volumes were examined. An existing empirical formula describing the evolution of the scour at a single pile in current or waves was extended to describe the scour at the pile breakwater under the action of multiple solitary waves, and new empirical coefficients were obtained by fitting the formula to the new experimental data to estimate the equilibrium scour depth. It appears that the maximum scour depth and the total scour volume are two reliable quantities for validation of numerical models developed for the scour around pile breakwaters under highly nonlinear wave conditions.

Keywords: sediment transport; solitary wave; shore protection; foundation safety

1. Introduction

Scour around structures built in coastal erodible bed is an important phenomenon that influences the foundation stability of various coastal structures. Vertical-pile or pile-group structures are commonly seen marine structures in engineering practice, such as offshore wind turbine monopiles, pile breakwaters, and slotted wave screens. The presence of such structures in a wave field changes the local flow pattern, creates

*Corresponding author contacts:
Email address: zhenhua@hawaii.edu (Zhenhua Huang)

a high flow velocity locally and enhances the turbulence intensity, which in turn amplifies the bed shear stress and enhances the local scour around vertical piles. Survivability of structures during extreme events such as tsunamis and storm surges is an important factor to consider when designing coastal structures. Field surveys and laboratory experiments have shown that the combined effect of the enhanced local scour and strong hydrodynamic loading is responsible for the failures of some coastal structures; however, modeling these extreme events in wave flume tests is a challenge because of the long spatial and temporal scales associated with these events [1–3]. Historically, solitary waves have been used to mimic tsunami waves in wave flume tests for their high repeatability in laboratory conditions.

There is a rich literature in the local scour around vertical-pile structures in steady currents or regular waves [4–9]. There are also studies on the tide-induced scour around vertical pile structures [10–12]. The complex interaction between near-field turbulence structures and sand grains effectively enhances bed shear stress, and has been studied experimentally and theoretically by Mattioli et al. [13] and Manes and Brocchini [14] for single vertical or horizontal piles. Scour develops when the bed shear stress, which is affected by the thickness of the bottom boundary layer [15], exceeds the critical bed shear stress. Both the near-bed turbulent flow condition and the bed roughness, which is related to the particle size distribution [16], can affect the thickness of the bottom boundary layer (see Part III of CEM [17]). For the scour around a single vertical pile in steady or oscillatory flow conditions, the main near-field turbulent flow feature that controls the scour around a vertical pile has been identified as the horseshoe vortex [18–20]: horseshoe vortex significantly enhances the bed shear stress around the structure [21]. Experimental observations of the steady-current induced scour around a single vertical pile and the flow around it have highlighted the geometric and dynamic relationships between the horseshoe vortex at equilibrium and the equilibrium scour hole: the horseshoe vortex is about 20% the size of the vertical pile at initial formation, and after the scour hole is deeper than 20% of the size of the pile, the primary horseshoe vortex grows linearly in size along with the increase of the scour depth and remains fully buried within the scour hole [22–24]. For a typical sand particle size distribution, the equilibrium scour depth around a single vertical pile can be predicted based on the assumption that at equilibrium, the maximum scour depth is similar to the size of the horseshoe vortex at the toe [14, 20]. Utilizing the method of phenomenology of turbulence and a canonical assumption that the characteristic length scale of the horseshoe vortex approximates the depth of the scour hole, theoretical prediction of the equilibrium scour depth under steady current condition has shown a close relationship between the scour profile and the horseshoe vortices [14]. At the equilibrium state, the horseshoe vortex size is similar to the size of the vertical pile, therefore the equilibrium scour depth in a steady flow over a sandy bed of typical grain size is in the range of 1.0 to $1.5D$ according to numerous experimental studies [11, 15, 25], where D is the diameter of the cylinder. For a single pile in pure waves or waves on a current, the equilibrium scour depth is known to be limited by the Keulegan-Carpenter (KC) number, which describes the relative

importance of the drag force over the inertia force acting on a body in an oscillatory flow. The equilibrium scour depth for single pile in pure waves or waves on a current is smaller than that in pure steady currents [8, 15, 21, 26].

Major relevant experimental studies in the literature are listed in Table A.1 in Appendix A. The main conclusions from the laboratory experiments investigating the scour around a standalone vertical circular cylinder in currents or regular waves with moderate to large KC numbers [8, 11, 15] are highlighted here: (i) for larger KC numbers, the horseshoe vortex induced by the local down-streaming and the lee-wake vortex is responsible for the local sediment suspension and the sediment removal around the vertical pile, and the equilibrium scour depth obtained under oscillatory flow conditions can approach that obtained under unidirectional current conditions [11]; (ii) for smaller KC numbers (for example, $KC < 1.0$), the scour is mainly attributed to the steady streaming effect [8]. The empirical formulas for predicting the evolution characteristics of the scour depth around a standalone vertical pile in waves and steady currents have been proposed by Sumer et al. [15].

Some experimental studies at a group of piles can also be found in the literature. The layout and gap of the piles in a group can greatly affect the scour at a group of piles. The pile layouts of major existing laboratory studies of the scour at a group of piles are summarized in Table A.2 in Appendix A. When the distance between pile is larger than a certain distance for a given layout, usually when $n = G/D > 2-4$ (where G is the gap size and n is the gap-diameter ratio [27–29]), the influence of neighboring piles disappears and all the knowledge obtained for a single pile can be applied to the local scour at an individual pile in a group. However, the local flow near a pile can be affected by the presence of neighboring piles when the distance between piles is smaller than a critical distance [27, 28, 30, 31]; the value of this critical distance is known to be affected by the incoming flow condition and the layout of the piles [32]. For example, for side-by-side arrangements, the scour depth first increases with reducing the gap size between adjacent piles, reaches a maximum at $n \approx 0.3$, decreases as the gap size continues to reduce, and eventually the scour depth approaches that for a single pile with an equivalent diameter for the group when the gap size is very small [33]. For a pile breakwater consisting of a row of closely spaced slender piles in regular waves, the scour depth is strongly related to two factors: (i) the ratio of the jet flow velocity in the gap and (ii) the fall velocity of the sediment particles. The scour depth around the closely spaced piles in regular waves is in the range of 1.5 to 2 times the diameter of piles [34], which exceeds the maximum values observed for a single pile in steady currents. It is worth noticing that in the experiment of Hayashi et al. [34], the sediment particles are artificial particles instead of natural quartz sand and their paper reports only equilibrium scour depth.

Table A.2 in Appendix A shows that the pile-group layouts in all but one existing studies are three-dimensional. In particular, Sumer and Fredsøe [33] conducted a set laboratory tests investigating the scour around three-dimensional circular pile groups in regular waves. Several three-dimensional group layouts, including side-by-side, tandem and staggered pile groups, have been tested, and the gap-diameter ratios

ranging from n=0.01 to 3.0 have been examined. For smaller gap-diameter ratios (for example, for a gap-diameter ratio of $n < 0.1$), the pile group behaves like a single pile with an increased diameter; for larger gap-diameter ratios (say, $n > 2$), the influence of neighboring piles diminishes and the piles in the pile group behaved like standalone piles. For similar gap-diameter ratios ($n < 0.5$), a row of two piles in a side-by-side arrangement have shallower equilibrium scour depth compared to a row of three piles in a side-by-side arrangement, which might be due to the influence of the enlarged area of bed exposure to the pile group in the latter case. Even though Sumer and Fredsøe [33] have highlighted the difference between standalone pile and pile group in wave conditions, no information is provided for (i) highly nonlinear waves such as solitary waves and (ii) possible end effects of on the middle piles in a three-dimensional pile group of finite width.

Compared to the rich literature in the local scour around vertical piles under steady currents or regular waves, research on local scour at pile structures due to highly nonlinear waves such as solitary waves is scarce [35, 36]. Tonkin et al. [1] conducted laboratory tests investigating the local scour at a standalone vertical circular pile on a 1:20 slope under the action of solitary waves. Nakamura et al. [2] reported an experimental study of the solitary-wave induced local scour at a square pile sitting on a dry sandy beach close to still water shoreline. These experimental results have shown that the scour depth around the structure is related to the incident solitary wave height and the depth of the pile foundation, and some of the key scour patterns observed in post-tsunami field survey in Kalapakkon (India) and Banda Aceh (Indonesia) after the 2004 Sumatra-Andaman earthquake tsunami can be reproduced in the experiment. Experimental investigations has also found that pore pressure can induce a reduction in the effective stress [1, 36].

Local scour around vertical structures due to solitary waves is different from that due to steady currents or tides because the flow associated with a solitary wave has a much shorter time scale. There are significant changes in both the flow speed and depth in a relatively short period of time during the passage of a solitary wave. It is also different from that due to regular waves or oscillatory flows in that solitary waves are not periodic and lack reverse flows. Because the unsteady velocity of a solitary wave is unidirectional, there is no periodic two-way formation and destruction of the wake vortex and horseshoe vortices. A major difference between a three-dimensional pile group (or a single pile) and a pile breakwater (a two-dimensional pile group) is the blockage effect of the pile breakwater and the resulting strong jet flows in the gaps in a pile breakwater, which are expected to enhance the scour depth and shorten the time required to reach the equilibrium. Compared to a rich literature in the hydrodynamics of pile breakwaters [e.g., 37–39], less research has been done on the scour at pile breakwaters, which is important for the survivability of such coastal structures during extreme events such as tsunamis and storm surges.

The motivation of the present work was to study the scour process around a pile breakwater in a tsunami event. Solitary waves were used in this study as a proxy for tsunami waves due mainly to the high repeatability of solitary waves in

laboratory conditions. A description of the pile breakwater, experimental setup and test conditions is given in Section 2. Effects of wave height and water depth on the evolution of scour-hole pattern and scour-hole characteristics are discussed in Section 3. An analysis of the equilibrium scour depth is presented in Section 4. Main conclusions are drawn in Section 6.

2. The pile breakwater model, experimental setup and test conditions

2.1. Experimental setup

The pile breakwater model is shown in Fig 1. The circular pile breakwater model was made of perspex, consisting of a base plate, a top plate, and four circular tubes. The width of the model was 0.495 m, slightly smaller than that of the wave flume. The diameter of each circular pile D was 0.09 m. The width of the breakwater model was 0.5 m (the same as the width of the wave flume), and the width of the gap between two adjacent piles was 3.5 cm, resulting in a gap-to-diameter ratio of 0.39. Each vertical circular pile had two sections: a lower section and an upper section. The lower section had a height of 25 cm, and was firmly glued to the base plate; the upper section was connected to the lower section via a specially designed "cross-connector". A top plate was mounted to the top of the circular piles. The overall height of the model was the same as the flume depth so that the top plate could be firmly fixed onto the side rails of the wave flume using clamps. The use of clamps and cross-connectors was to ensure that: (i) the model was stiff enough to withstand wave loading, and (ii) the upper section could be easily disassembled without causing disturbance to the sand bed for bed profile measurement using a laser scanner.

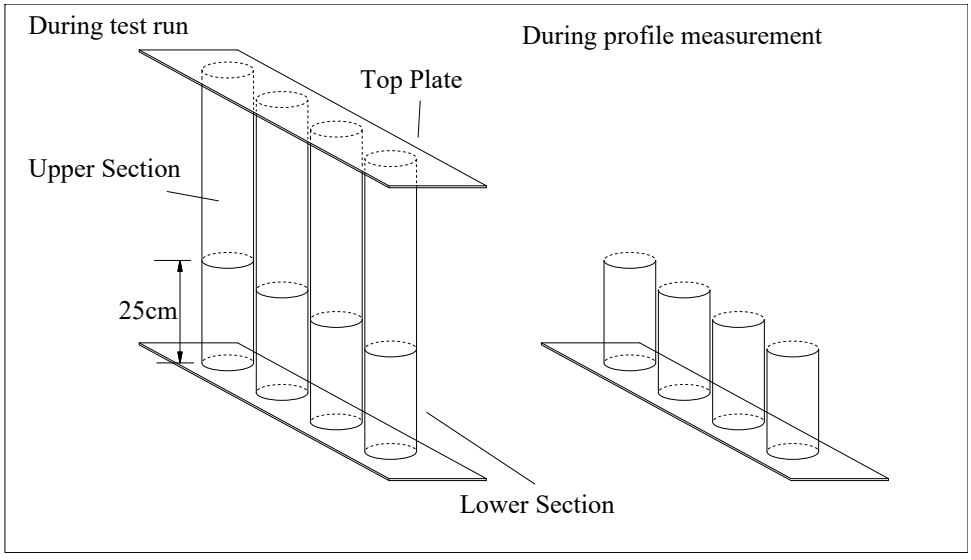

Fig. 1: Sketch of the pile breakwater model. Left panel shows the model with the top section when running solitary waves, and the right panel shows the model without the top section for measuring the bed profile using the underwater laser scanner.

The model shown in Fig. 1 was tested in a wave flume in the Hydraulic Laboratory at the Changsha University of Science and Technology, China. A sketch of the experimental set up is shown in Fig 2. The dimensions of the wave flume were 40-m long, 0.5-m wide and 0.8-m deep. At one end of the wave flume, a piston type wave maker was installed; at the other end of the wave flume, a 1 : 10 wave absorbing beach was installed to reduce wave reflection. The wave absorbing beach was covered by a layer of porous material to further reduce wave reflection from the beach. The weak reflected wave coming from the absorbing beach was not able to cause any change in the bed profile in this study. In order to reduce multiple reflections of the generated solitary wave between the paddle of the wave maker and the breakwater model, a special wave-blocking plate was designed and installed at 8 m from the paddle. The operation and effect of the wave-blocking plate will be further explained later in this section.

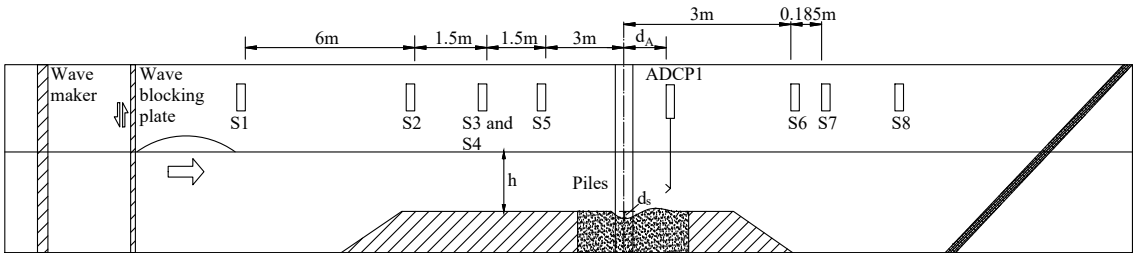

Fig. 2: Sketch of experimental setup

In the experiment, the pile breakwater model was placed 22.6 m from the wave generator. To create a 1.9-m long and 0.2-m deep sand bed (or sand pit) for installation of the breakwater model, two false bottoms were used. The false bottom on the up-wave side of the sand pit was 20-cm high, having a 1 : 5 slope and a flat section; the total length of the false bottom on the up-wave side of the pile breakwater was 5.8 m. The length of the sand bed on the up-wave side of the model was 0.8 m. The length of the sand bed on the down-wave side of the model was 1.2 m, which was long enough for the scour hole to develop without being interfered by the end on the down-wave side. The total length of the elevated sand bed and the false bottom on the up-wave side of the model was 6.5-m long, which allowed for the incident wave to deform and stabilize before reaching the model. The sand pit was filled with natural beach sand of diameter $d_{50} = 0.25$ mm and a specific weight of $\gamma = 2.6$. After finishing each test run, the sand bed was re-prepared to a flat bed condition using a perspex sheet board.

Referring to Fig. 2, eight Ultralab ultrasound sensors (S1 to S8) were used to monitor the water surface. S1 was placed 12 m away from the breakwater model on the up-wave side to measure the incident wave; S2, S3, and S4 were placed 6 m, 4.5 m and 3 m away from the breakwater model on the up-wave side to monitor the wave deformation and reflection by the false bottom and the model; S5 was placed 4.5 m

away from the breakwater model on the up-wave side, parallel to S3 with a distance of 0.15 m in between to monitor the lateral variation of the waves inside the flume; S6 and S7 were placed 3 m and 3.185 m away from the breakwater model on the down-wave side, respectively, to monitor the wave reflected from the wave absorbing beach; S8 was used as a redundant gauge.

It must be noted that in this experiment the water depth h is specified as the one measured from the false bottom, so the actual water depth at the wave maker is the water depth h plus the height of the false bottom (20 cm), as shown in Fig 2.

Because the wave-making paddle itself is almost perfectly reflective, multiple reflections exist between the model and the paddle if no special measure is implemented to remove the wave reflection from the paddle. To reduce the reflected wave coming from the wave paddle side, a special wave blocking system was designed (refer to Fig. 2) and installed, which prevented the re-reflection by the wave paddle of a solitary wave coming from the model side. This wave blocking system is operated in the following way:

1. The wave blocking plate is first lift from water to a height that allows the passage of the generated solitary wave.
2. After the water surface inside the wave flume is free from any sensible residual waves (this usually means allowing a waiting time of at least 4 minutes), a solitary wave is generated. This is to ensure the quality and repeatability of the solitary waves generated under the same test condition.
3. When a solitary wave coming from the model side has just past the wave blocking plate, the wave blocking plate is lowered down immediately so that this reflected solitary wave is trapped between the wave paddle and the wave blocking plate. This can prevent this solitary wave from multiple reflections between the model and the wave paddle.
4. Only after the solitary wave trapped between the wave paddle and the wave blocking plate diminishes can the wave blocking plate be lifted again for generating the next solitary wave.

It will be shown in Section 3.2 that the incoming solitary wave will be reflected by both the false bottom and the model, but the wave blocking plate can only be operated to trap one of them. The reflection coefficient at the wave-generator end is less than 0.15 if the wave-blocking plate is operated to trap the solitary wave reflected by the model (see Section 3.2 for model details).

In order to measure the three-dimensional sand bed profile near the pile model, an underwater laser scanner (2GRobotics ULS-100®) was used to scan the sand bed profile. Prior to actual measurement, the upper section of the model was removed so that only the lower section of the model was left in the sand bed (see the right panel of Fig. 1). Due to the limitation in the size of the area which the scanner can cover, the entire scanned bed profile was a combination of $12 - 18$ scanned patches. In order to ensure the accuracy of the final profile after combining measurement patches, the lateral scanner positions were precisely determined using a high-precision

measurement bridge and the longitudinal positions of the bridge were determined on a ruler with a spatial accuracy of less than 1 mm. Fig. 3 shows a view of the underwater laser scanner during one test run.

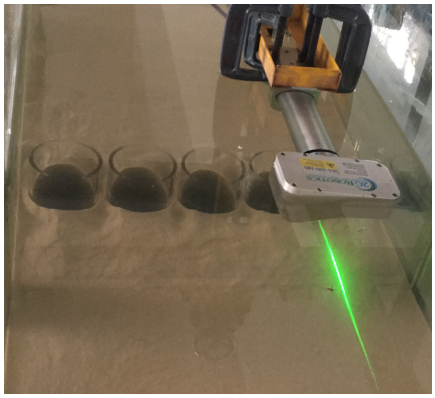

Fig. 3: A view of the laser scanner measuring bed profile near the row of disassembled piles.

Close to the narrow gaps formed by the piles, the accuracy of the underwater laser scanner deteriorates because of the inevitable "laser footprint error", which is due to the added refraction and reflection of the laser beam from the model. The "laser footprint error" or "edge effect" may be induced when scanning sharp edges, which may lead to erroneous measurements near sharp edges, such as the edge of the lower portion of the pile model. In the present experiment, another source of error may also be present, which is the refraction of laser beams through the Perspex layer of the pile model. To provide data in the regions affected by the "laser footprint error", a point probe was used in the experiment to supplement data inside the narrow gaps by measuring the scour depth at fixed locations inside the gap.

In the following, we describe how these two sources of error occur when measuring the bed profile near the edge of the lower portion of a pile and in the region between two piles.

As illustrated in Fig. 4, the laser scanner has two optical parts: one is the laser emitter (shown in the figure as the right arm of the laser scanner), and the other is the receiver lens, which is the left arm of the laser scanner. The laser beam emitted from the scanner is labeled as beam A. We illustrate here the two sources of error based on the two scenarios shown in Fig. 4.

The first scenario is shown in the left panel of Fig. 4. When the laser beam A reaches the bed profile, the reflected light as seen by the receiver window is a combination of the refracted beam C and the reflected beam B coming from the top edge of the lower portion of the pile. Therefore, the scanned profile in the small shadowed region is erroneous, with inaccurate points from the refracted beam C and wrong points from the reflected beam B. The other scenario is shown in the right panel of Fig. 4. When the laser beam A from the laser emitter reaches the bed profile, and the reflected beam B reaches the receiver lens without being blocked, refracted or

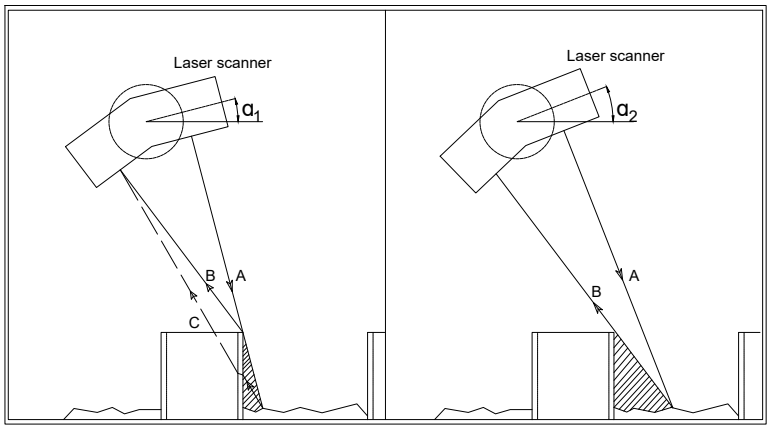

Fig. 4: An illustration of the optical path of the laser scanner near the lower portion of the piles.

reflected by the pile; in this scenario it can provide reliable measurements. It is clear that the region in the shadow is erroneous. As the scour hole gets deeper, the size of the shadowed region increases.

2.2. Test conditions and procedure

Solitary waves were used in this study as a proxy for tsunami waves due mainly to the high repeatability of solitary waves generated in laboratory conditions. Solitary waves as a proxy for tsunami waves are able to capture some of the physical phenomenon found in a typical tsunami event [35, 40–42], but they also suffer from scale issues: compared to real tsunamis, solitary waves tend to have too high non-linearity and are much shorter in both temporal and spatial scales. Because it is not possible to generate a tsunami in a wave flume that satisfies all similarity requirements, scale distortion has to be accepted in experimental studies of tsunami-related problems, which is especially true for studying tsunami-induced sediment transport: it is impossible to scale tsunamis properly in the laboratory such that sensible sediment transport can be generated [40, 43]. To partially solve this issue, in some recent studies of tsunami-induced local scours, multiple solitary waves have been used to compensate for the short duration due to the use of solitary waves [43, 44]. Even though dam-break waves or moving bores have also been used in the past as a proxy for tsunamis to study tsunami-induced runup [45, 46], using multiple dam-break waves or moving bores to study tsunami-induced scours may pose a problem in the repeatability of the results since they are much less controllable than solitary waves. It is remarked here that Nakamura et al. [2] have reported that solitary waves are able to capture tsunami-wave induced sediment scour patterns, indicating that application of solitary waves to study tsunami-induced scour is still at least plausible.

A summary of the test conditions is given in Table 1, where u_* is the shear velocity, θ is the Shields parameter calculated using u_*, and the equivalent period T_s

for a solitary wave [47, 48] is calculated by

$$T_s = 4\pi\sqrt{\frac{h^3}{3gH(h+H)}}, \tag{1}$$

where h is the local water depth at the model, H the incident wave height, and g the gravitational acceleration. The calculation of the shear velocity u_* will be given in Section 4.

Table 1: Test Conditions

Case	h(m)	H(m)	h/D	H/D	T_s (s)	u_* (m/s)	R_e	θ
1	0.25	0.06	2.778	0.667	2.12	0.030	3.08×10^4	0.227
2	0.25	0.04	2.778	0.444	2.69	0.024	2.16×10^4	0.142
3	0.25	0.08	2.778	0.889	1.78	0.034	3.85×10^4	0.277
4	0.23	0.06	2.556	0.667	1.94	0.031	3.18×10^4	0.231
5	0.20	0.06	2.222	0.667	1.66	0.031	3.51×10^4	0.241

In Table 1 the Reynolds number Re is defined as

$$Re = \frac{U_m D}{\nu}, \tag{2}$$

where D is the diameter of the pile and U_m is the maximum velocity in a solitary wave, calculated using the solitary wave theory of Grimshaw [49]. The wave heights listed in Table 1 are the target wave heights used to prepare input files for the wave maker; the actual measured incident wave height may slightly differ from the target value, within a maximum difference of 5% for all test conditions.

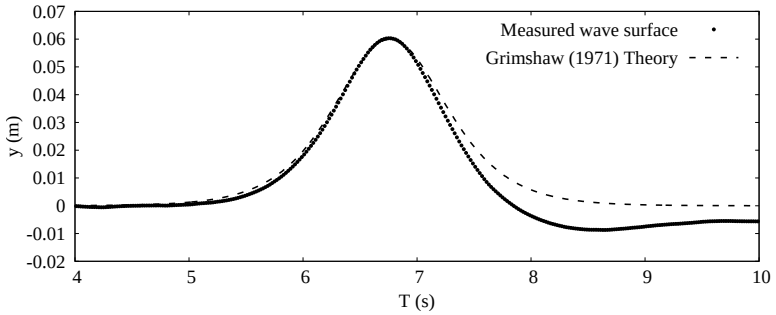

Fig. 5: A comparison of the measured surface displacement and the theoretical surface displacement of Grimshaw [49].

The typical water depth for the prototype pile breakwater is slightly less than 10 m. Take h=10 m for prototypes and h=0.25 m for the model as an example, the geometrical scale is about 40. The maximum height of tsunami targeted in this study is about 3.2 m at a water depth of 10 m.

3. Results and discussion

This section presents the experimental results in dimensionless forms: all lengths are non-dimensionalized using pile diameter D, all time dimensions are non-dimensionalized using the following time scale T_0 [15]

$$T_0 = \frac{D^2}{[g(\gamma - 1)d^3]^{1/2}}, \tag{3}$$

and all volumes are non-dimensionalized using $\pi D^3/4$.

3.1. Measured surface elevations

An example of the temporal variation of the water surface measured by the Ultralab sensor S1 for a target wave height of $H/D = 0.667$ is shown in Fig. 5, where the theoretical profile obtained using the solitary wave theory of Grimshaw [49] is also included for comparison. It can be seen that the measured wave front agrees well with theoretical solitary wave profile; however, the tail of the measured wave is slightly steeper than the theoretical one, and a slight set-down in the surface elevation can be observed after the wave peak passes S_1. These minor differences between the measured solitary waves and the theoretical ones have also been observed in other experimental studies involving solitary waves [3, 48, 50]. Fig. 6 shows one example of the surface displacements measured by wave gauges S1, S3, and S5 for h/D=2.556 and H/D=0.667. An increase of 6.1% in wave height can be observed from S1 to S5. The shoaling of the incident solitary wave on the false bottom makes the wave front slightly steeper and the back of the wave slightly gentler.

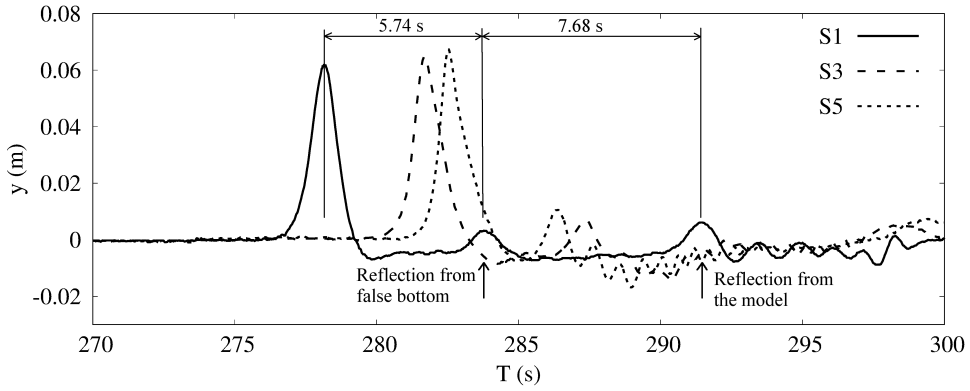

Fig. 6: Sample time series of a solitary wave recorded by S1, S3 and S5 installed in front of the model.

3.2. Reflections at the two ends of the wave flume

At the location of the wave gauge S1, two small reflected waves can be observed after the passage of the main solitary wave: the wave reflected by the false bottom and the wave reflected by the test model. A simple calculation based on the speeds of the solitary waves and the distances of the false bottom and the model to the wave paddle and the blocking gate can show that the wave blocking gate cannot block both reflected waves. For all test conditions, the height of the wave reflected by the false bottom was smaller than that by the model; therefore, the wave blocking gate was operated in the experiment to block the solitary wave reflected by the model. As a result, the reflection coefficient of the wave blocking plate should be determined by the reflection of the wave reflected by the false bottom, not by the reflection of the wave reflected by the model. Assuming that the wave reflected by the false bottom experiences a perfect reflection at the wave paddle, the reflection coefficients at the wave-generator end for all test conditions were in the range of 0.113 and 0.152, which were smaller than the reflection coefficients at the end of the wave-absorbing slope end.

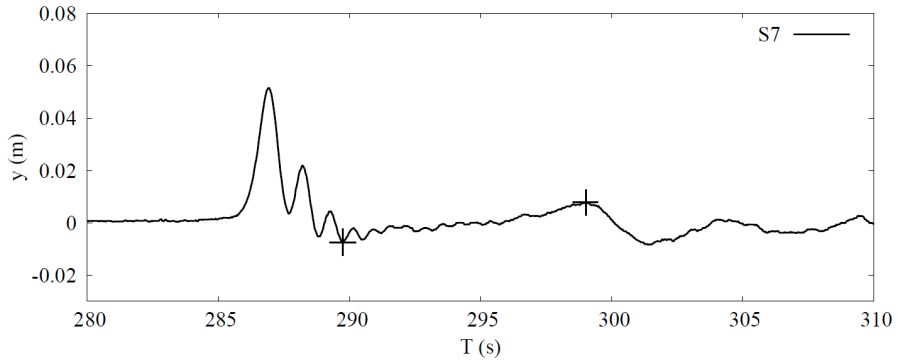

Fig. 7: An example of water surface elevation behind the model measured by S7. The two + signs indicate the locations used to determine the height of the reflected wave.

Fig. 7 shows one example of the time series of the surface displacement measured at wave gauge S7 for h/D=2.778 and H/D=0.667. The weak reflected wave is significantly elongated compared to the incident solitary wave. Defining the height of the reflected wave as the difference between the lowest elevation and the highest elevation immediately after the main solitary wave passes the wave gauge S7, we found that the heights of the reflected solitary waves were in the range of 0.2 and 0.3 for all tested waves.

Using the long wave theory to estimate the peak velocity and the wave friction factor [51] to estimate the friction velocity, we find that the Shields parameter associated with the waves reflected from both the wave-generator end and the wave-absorbing end are too small to cause any sensible scour according to the experimental results of Sumer and Fredsøe [33] for two/three side-by-side piles with a similar gap-diameter ratio in regular waves.

3.3. Change of the bed profile measured by laser scanner

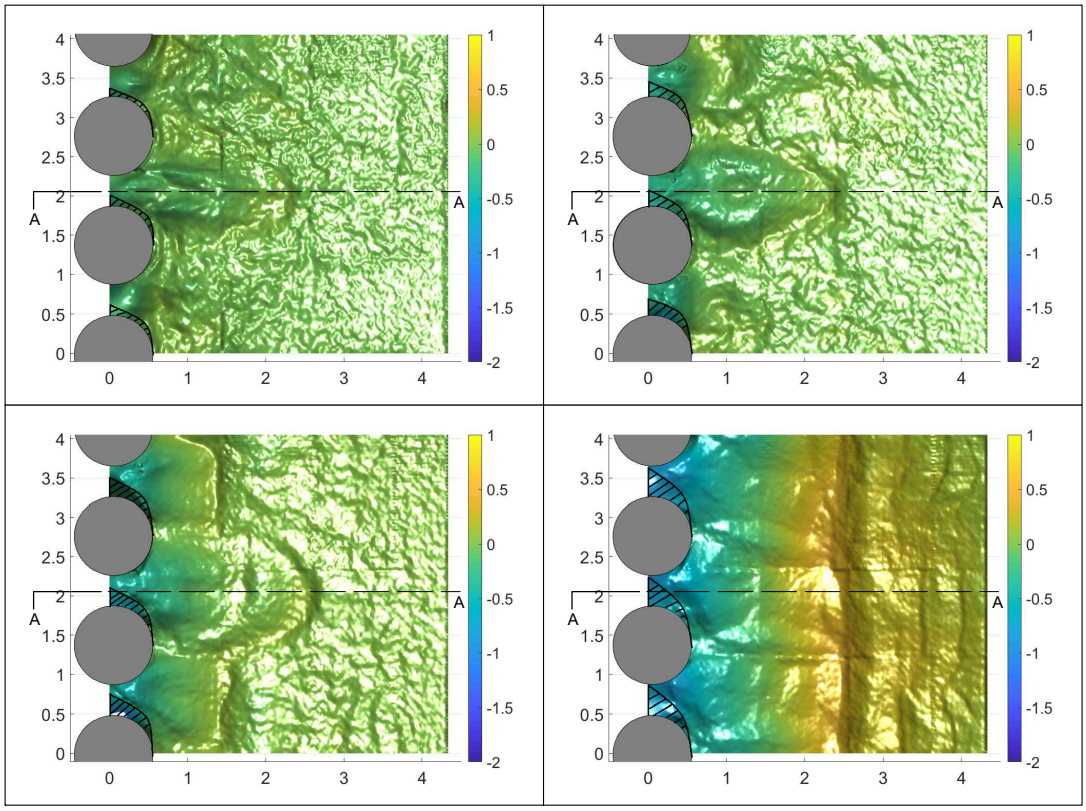

Fig. 8: Samples of scanned bed profiles taken for Case 2, measured after 7 (top left), 13 (top right), 24 (bottom left) and 99 (bottom right) waves. The shaded regions are affected by the "laser footprint error". The horizontal axis is x/D and the vertical axis is y/D. All lengths are normalized by D.

Fig. 8 shows an example of the scanned three-dimensional bed profile on the down-wave side of the pile breakwater model for Case 2 listed in Table 1. The scanned region can only reveal the scour patterns away from the two side walls. The scanned bed profile in the regions between the two ends of the pile breakwater model and the two side walls may be affected by the interference between the side walls and the laser beam, and thus not included in Fig 8. In the early stages of the scour process (e.g., after running 7, 13 and 24 waves for the case shown in Fig. 8), the scour at the central gap is slightly different from that at the adjacent gap on each side, and the difference in the scour patterns at the three gaps significantly reduces at the later stage of the scour process (after running 99 waves). Because the bed profile in the gap between two piles could not be accurately measured using the laser scanner, a point gauge was also used to measure the scour depths at nine selected locations between the two piles: three locations were on the A-A transect shown in Fig. 8, and the other six on the two sides of the transect A-A with three on each side.

Technically, the A-A transect should coincide with the center line of the wave flume. The scour profiles along the A-A transect are shown in Fig. 9 for the four

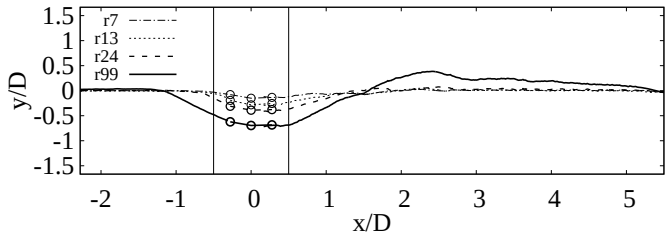

Fig. 9: 2D bed profiles for Case 2, taken at the transect A-A shown in Fig 8. Note that the symbols "o" represent point gauge measurements.

instants shown in Fig. 8. It can be seen that the point-gauge data merge well with the scanned profiles. The scour hole deepens with increasing number of solitary waves. Even though solitary wave has a unidirectional velocity, the sand can be removed on both the up-wave and down-wave sides of the pile breakwater; however, the sand deposits mainly on the down-wave side of the breakwater, eventually forming a sandbar on the down-wave side of the pile breakwater. After running 99 waves, the bed profile along the A-A transect is characterized by a scour hole at the gap and a sandbar on the down-wave side of the pile breakwater.

There are two types of asymmetric features that can be observed in the scour profile near the pile breakwater model as shown in Fig. 8: (i) the asymmetry of the scour profile in the longitudinal direction (i.e., the direction of wave propagation), and (ii) the asymmetry of the scour profile in the lateral direction (i.e., the direction parallel to the wave crest). The reasons for these two types of asymmetry are explained as follows:

1. For the asymmetry of the scour profile in the longitudinal direction, the main contributing factor is the asymmetric nature of the flow velocity for solitary waves. Unlike regular waves where the flow velocity is oscillatory, the velocity field of a solitary wave is mainly unidirectional. As a result, the horseshoe vortex system on the up-wave side and a turbulent wake on the down-wave side can be formed during the wave passage. The horseshoe vortex is responsible for the scour on the up-wave side, while the turbulent wake is mainly responsible for the scour on the down-wave side. Because the scour mechanisms are different on the two sides of the breakwater, the scour profile is asymmetric.
2. For the asymmetry in the lateral direction, two factors may have contributed to it. First, the asymmetry found in the gaps are mainly due to the measurement error caused by the "laser footprint error". Second, the slight difference on the two sides of the transect A-A is due mainly to the asymmetric nature of the complex turbulent wake flow generated by the jet flow in the gap.

Because of the 3D features of scour holes at the pile breakwater, we stress two points here:

1. the conservation of mass cannot be evaluated based on the 2D bed profile along the A-A transect, and

2. the maximum scour depth in a scour hole between two piles may or may not occur on the A-A transect.

For later discussion of our experimental results, Fig. 10 shows a definition sketch of the important dimensions that characterize the scour profile near a pile breakwater.

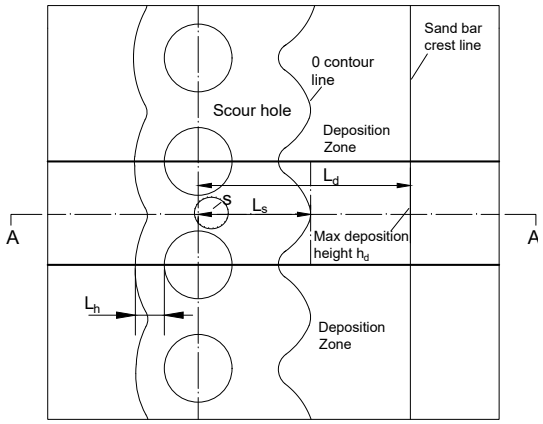

Fig. 10: A sketch showing definitions of four key characteristic dimensions. The maximum scour hole depth is determined in a small region between two piles, as shown by the dashed oval circle. Not drawn to scale.

To discuss effects of wave height and water depth on bed-profile characteristic dimensions, the following four key characteristic dimensions of a scoured bed profile are defined in Fig. 10:

1. The maximum scour depth s is defined as the deepest location in the scour hole, usually located in the gap and having a slight shift toward the down-wave direction.
2. The length of the scour hole on the down-wave side of the pile breakwater L_s is defined as the distance between the center axis of the pile breakwater to the first zero-contour line on the down-wave side of the pile breakwater.
3. The maximum deposition height h_d is defined as the highest point of the deposition region on the down-wave side of the scour hole. When a sandbar can be clearly identified at the later stage of the scour process, the maximum deposition height is the sandbar height.
4. The length of the scour hole on the up-wave side of the pile breakwater L_h is defined as the distance between the up-wave edge of the pile breakwater to the first zero-contour line on the up-wave side of the pile breakwater.

When discussing these characteristic dimensions in this section and the scour and deposition volumes in the next section, we only focus on the scour profile within the two bold lines (between the central axis of the 2nd pile and the central axis of the 3rd pile), as indicated in Fig. 10.

The repeatability of the experiment was verified by carrying out repeating tests for the case of $h/D = 2.778$ and $H/D = 0.889$, as reported in Appendix B, where an

uncertainty analysis was performed on the measured characteristic dimensions using this set of repeating tests. Only the results with low uncertainty are presented and discussed in the rest of this section. Error bars are included in the figures only for $H//D$=0.889 and h/D=2.778 under which the repeatability tests were performed.

3.4. Effect of water depth and wave height on the 3D scour profile

The scour at the pile breakwater is induced by the horseshoe vortex on the up-wave side and the jet flow through the gap between two adjacent piles on the down-wave side. The evolution of the 3D scour profile [in the region between the two thick horizontal lines in Fig. (10)] with the number of solitary waves passed is shown in Fig. 11 for H/D=0.444 and h/D= 2.778. The scour profiles shown in Fig. 11 are the changes of the bed elevation obtained by subtracting the initial bed profile from the scoured bed profiles caused by solitary waves passing the pile breakwater. The evolution of the scour profile is characterized by two stages. In the early stages, the scour-hole depth contours are characterized by 3D U-shaped contour lines; in these stages, the scour hole deepens with increasing number of solitary waves passed, and the scour hole formed near the gap has not connected with the neighboring scour holes on the two sides. At the later stage of the scour process (after running 99 waves), the scour hole gradually merges with neighboring scour holes, and the depth contour lines gradually straighten, and eventually a sandbar forms some distance on the down-wave side of the scour hole. Between the scour hole and the sandbar there exists a zero-contour line, which separates the scour hole and the sandbar.

Fig. 12 shows the evolution of the 3D scour profile [in the region between the two thick horizontal lines in Fig. (10)] for H/D= 0.667 and h/D= 2.778. Comparing Figs. 12 and 11, conclusions similar to those for Fig. 11 can be drawn, except that the time required for the scour holes to connect with their neighboring sour holes reduces with increasing wave height.

The time required for the scour hole to reach its equilibrium state will be discussed later in Section 4, where it will be shown that after running 99 waves the scour hole can reach its near-equilibrium state. At the near-equilibrium state, the slope at the edge of the scour hole is expected to approach the angle of repose, and the location of the zero-contour line representing the edge of the scour hole is expected to have less measurement error as compared to that at the initial stage of the scour process (refer to Appendix B for details).

The scour hole patterns for the tested three water depths (not included in the paper) are all similar, with only a minor difference in the scour depth.

3.5. Effects of wave height and water depth on the characteristics of the scoured bed profile

Before presenting the experimental results on the characteristics of the scoured bed profile, the uncertainty estimation of the experimental results is first discussed here. To address the uncertainty in these four characteristic dimensions shown in Fig 10, repeating tests were performed under the same test condition: H/D=0.889 and

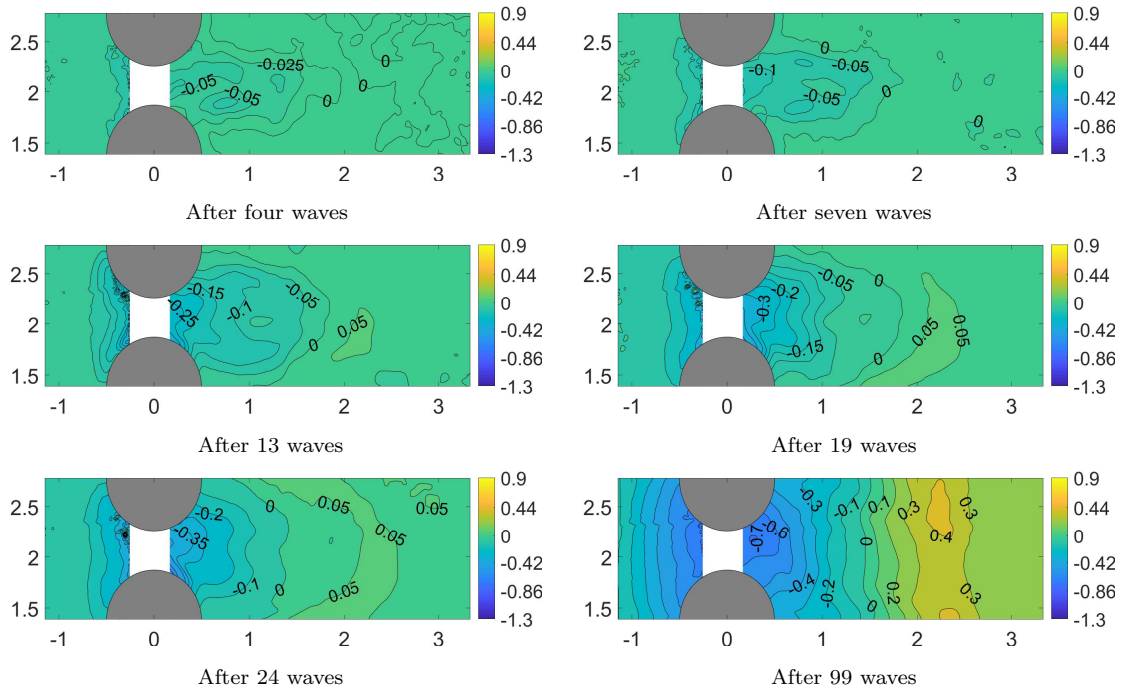

Fig. 11: Change of the 3D scour profile for H/D= 0.444 and h/D = 2.778. The regions that are affected by the "laser footprint error" are not marked out as in Fig. 8. The horizontal axis is x/D and the vertical axis is y/D. All lengths have been normalized by D.

h/D=0.278. An analysis of the source of uncertainty and the results with error bars for this set of repeating tests are included in Appendix B. In the experiment, the main source of uncertainty came from the preparation of the initial bed profile, which affected the determination of L_s and L_h in the early stages of the scour process. This is because these two quantities need to be determined by the zero-contour lines which can be strongly affected by the fine turbulent flow structures associated with the initial bed profile in the early stages of the scour process. The uncertainties in the scour and deposition sand volumes, maximum scour depth and maximum deposition height were found in the uncertainty analysis to be very small after running two waves. The uncertainties in the measured L_s and L_h were found to be small only after running 19 waves and 99 waves, respectively. Therefore, the results of the measured L_s before 19 waves are not included in the following discussion. For L_h, only the results obtained after running 99 waves are given in Table 3 where the measured key characteristics of the final bed profile are summarized.

Fig. 13 shows the evolution of sand deposition height, maximum scour-hole depth and the length of the scour hole on the down-wave side of the pile breakwater for three different wave heights (H/D = 0.444, 0.667 and 0.889) and a fixed water depth of h/D =2.778. The top panel of Fig. 13 shows that the scour hole depth s/D increases with the number of solitary waves passed, and a larger wave height generally results in a deeper scour hole. Because the dimensionless scour hole depth s/D is still less

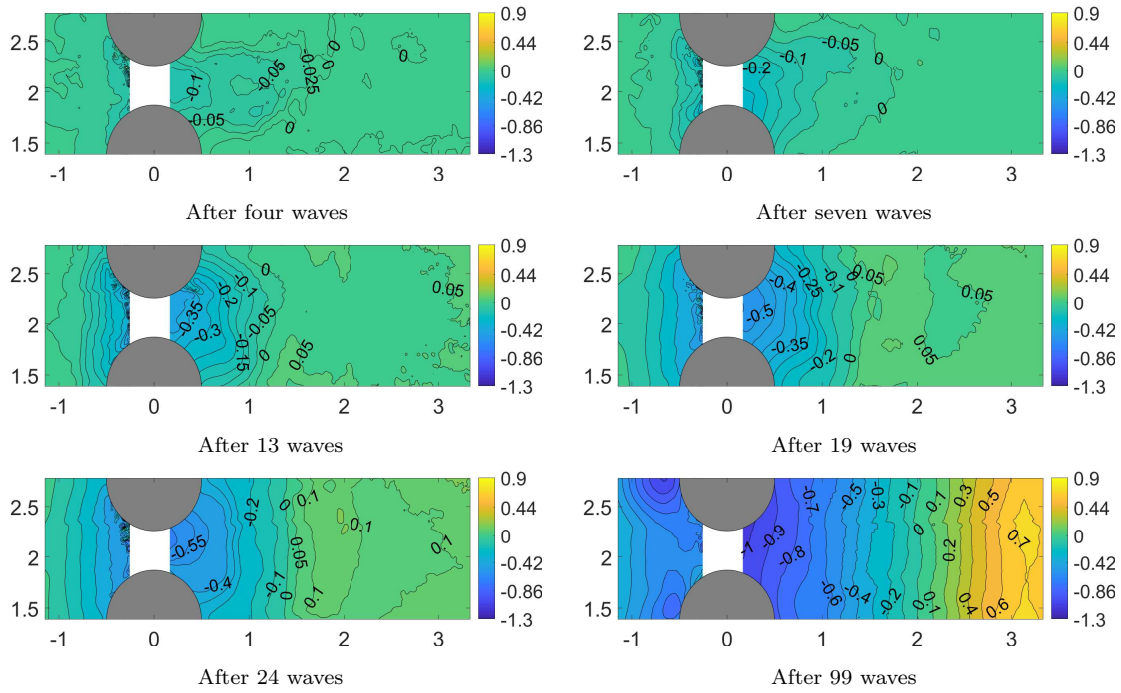

Fig. 12: Change of the 3D scour profile for H/D=0.667 and h/D = 2.778. The regions that are affected by the "laser footprint error" are not marked out as in Fig. 8. The horizontal axis is x/D and the vertical axis is y/D. All lengths have been normalized by D.

than 0.22 in the initial stages of the scour process (say, before running 10 waves), and the slight difference in the initial bed profiles for different test runs may have contributed to minor measurement errors observed in the initial stages of the scour process. As expected, the influence of the slight difference in the initial bed profiles for different test runs gradually diminishes with the development of the scour hole. The middle panel of Fig. 13 shows that the sand deposition height h_d/D increases with the number of solitary waves passing the pile breakwater and the sand deposition height increases with increasing solitary wave height. The measured sand deposition heights for H/D=0.667 are slightly higher than those for H/D=0.889, due possibly to the slight difference in the initial bed profiles for different test runs. For the scour hole length L_s/D shown in the bottom panel of Fig. 13, the uncertainty in L_s/D is small enough after running 19 solitary waves so that a correlation between the wave height and the scour-hole length can be observed: a higher wave height resulted in a longer scour-hole length.

Fig. 14 shows the measured maximum scour depth, maximum sand deposition height, and the length of the scour hole for three different water depths (h/D = 2.222, 2.556, and 2.778) and a fixed wave height of H/D=0.667. As expected, both the maximum scour hole depth s/D and the maximum deposition height h_d/D increase with increasing number of solitary waves passed. It can be seen that both the maximum scour hole depth and the maximum deposition height are not significantly

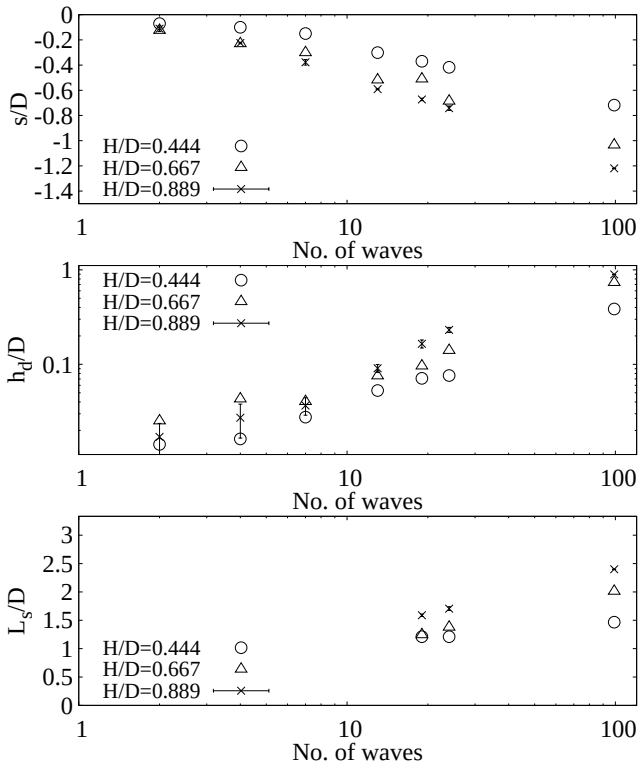

Fig. 13: The measured maximum scour depth (top panel), maximum deposition height (middle panel), and length of the scour hole (bottom panel) for three wave heights and a fixed water depth of h/D=2.778. The values of L_s/D for the first 13 waves are not included due to the high uncertainty associated with the preparation of the initial bed profiles. Error bars are included for H/D=0.889.

affected by the three water depths examined in this study. On the up-wave side of the pile breakwater, L_h/D indicates the horizontal size of the horseshoe vortex on the up-wave side of a pile [5]; this distance for the case shown in Fig. 11 is L_h/D = 1.222 after running 99 waves. The values of L_h/D after running 99 waves for all test conditions are summarized in Table 3.

It may be concluded from the results in this section that (i) sand deposition height and maximum scour depth are good characteristic dimensions for comparison with numerical simulations; and (ii) there may be large relative uncertainty in the measured scour-hole lengths L_s/D and L_h/D in the initial stages of the scour development, which makes them not good characteristic dimensions for comparison with numerical simulations.

3.6. Total scour and deposition volumes

Other two quantities that can be good candidates for comparison with numerical simulations are the total scour and deposition volumes. In consideration of the symmetry about the center line of the flume and possible effects of side walls, the volume of scoured sand (V_s) or the volume of sand deposition (V_d) are defined for the region

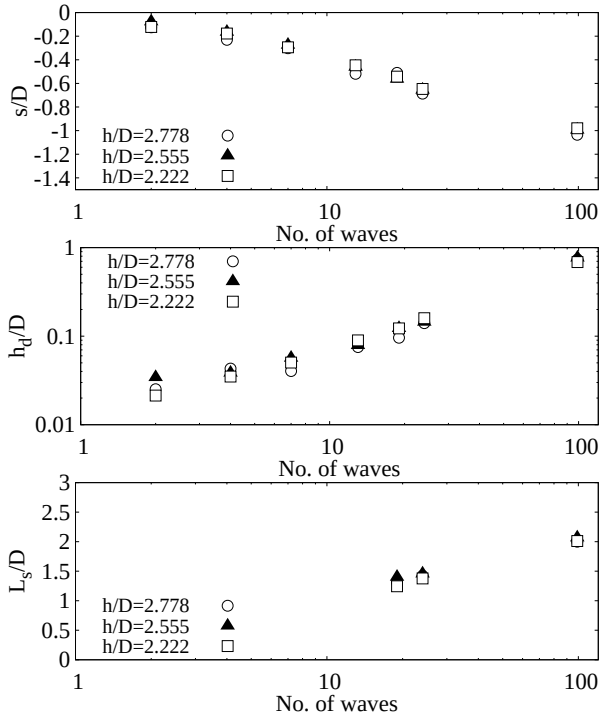

Fig. 14: The measured maximum scour depth (top panel), maximum deposition height (middle panel), and length of the scour hole (bottom panel) for three water depths and a fixed wave height of H/D=0.667. The values of L_s/D for the first 13 waves are not included due to the high uncertainty associated with the preparation of the initial bed profile.

within the two bold horizontal lines as shown in Fig. 10. Mathematically, V_s and V_d are calculated by

$$V_s = \int_\Omega s(x,y)dxdy, \quad V_d = \int_\Omega d(x,y)dxdy \tag{4}$$

where Ω is the area between the two bold horizontal lines as shown in Fig. 10, and $s(x,y)$ and $d(x,y)$ are the scour depth and deposition height at a given location (x,y), respectively. When calculating the scour and deposition volumes using Eq. (4), it is suggested that the integration should be carried out numerically on a mesh of size 1 mm in both directions.

Because of the possible measurement error due to the blockage of the laser beams by the lower sections of the piles, the region between two adjacent piles needs special treatment using symmetric data mapping and point gauge data mapping. Referring to Fig. 8, the data in the shaded region may have large error and thus should be discarded. The data in the shaded region can be filled in, through one of the two following methods, to compute the total scour volume:

1. Symmetric data mapping: If the data on the symmetrical side with respect to the central axis of the gap are available (e.g., the scenarios shown in the panels

(a) and (b) of Fig. 8), they can be used to replace the discarded data.

2. Point gauge data mapping: If the data on the symmetrical side with respect to the central axis of the gap are not available (e.g., the scenarios shown in the panels (c) and (d) of Fig. 8), the data obtained at nine points using a point gauge can be used to provide low-resolution data to replace the discarded data.

From our experimental results it was confirmed that the error induced by the data mapping described above was less than 5% of the overall scour or deposition volume in this experiment.

Fig. 15 shows the calculated total scour volumes for three different incident wave heights (H/D = 0.444, 0.667 and 0.889) and a fixed water depth of h/D = 2.778. The total scour volume increases with the number of solitary waves passed, and the incident wave height has a very significant effect on the calculated scour volume. For the smallest wave height (H/D = 0.444), the total scour volume reaches only $V_s = 0.144 \times [(1/4)\pi D^3]$ after 24 waves; while for the largest wave height (H/D = 0.889) the total scour volume reaches $V_s = 0.908 \times [(1/4)\pi D^3]$ after 24 waves, which is more than six times larger than that for the smallest wave height. For the case of H/D = 0.667, the total scour volume reaches $V_s = 0.551 \times [(1/4)\pi D^3]$ after 24 waves. The values of the scour volumes after 99 waves for all three wave heights are summarized in Table 3 in Section 5.

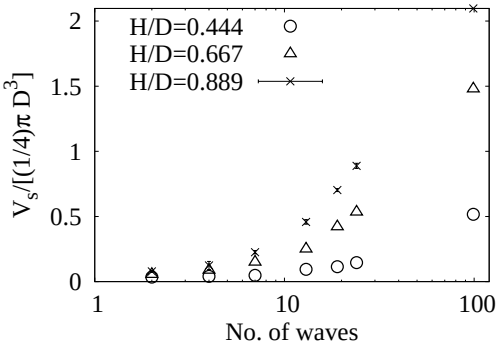

Fig. 15: The calculated total scour volumes for three different incident wave heights and a fixed water depth h/D = 2.778. Error bars are included for H/D=0.889.

Fig. 16 shows the calculated scour volumes for three water depths tested (h/D = 2.222, 2.556 and 2.778) and a fixed incident wave height of H/D = 0.667. The water depth does not seem to have a significant influence on the scour volume, which increases almost linearly with the number of solitary waves passed. The scour volume only slightly decreases with decreasing water depth after running 13 solitary waves. For all three water depths, the scour volume reaches about $V_s = 0.524 \times [(1/4)\pi D^3]$ after running 24 waves. The total scour volumes for all three water depths after 99 waves are summarized in Table 3 in Section 5.

Fig. 17 shows the calculated deposition volumes for three different incident wave heights and a fixed water depth of h/D=2.778. Similar to the calculated scour vol-

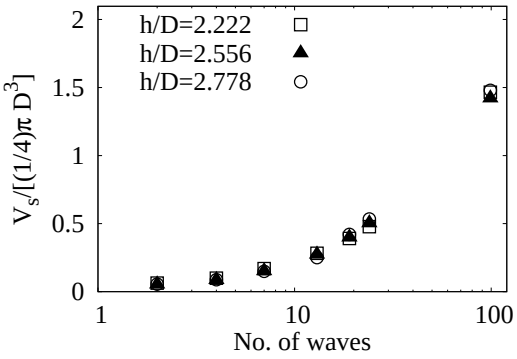

Fig. 16: The calculated total scour volumes for three water depths and a fixed wave height $H/D = 0.667$.

ume, the total deposition volume increases with both wave height and the number of solitary waves passed. Fig. 18 shows the calculated deposition volumes for three water depths and a fixed wave height of H/D=0.667. Again, water depth has insignificant influence on the calculated deposition volume, which increases with the number of solitary waves passed. The values of the total deposition volumes after 99 waves are summarized in Table 3 in Section 5.

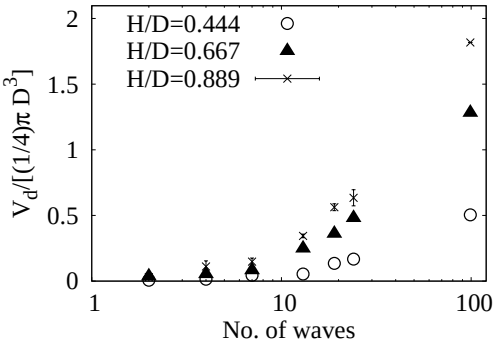

Fig. 17: The calculated deposition volumes for three incident wave heights and a fixed water depth of $h/D = 2.778$.

It can be found by comparing the total scour volumes and the corresponding total deposition volumes that the total deposition volume is slightly smaller than the scour volume. This is mainly because a certain amount of sand is transported outside the scanned area during the scour process.

4. A discussion of equilibrium scour depth

A number of empirical formulas exist for predicting the time development of the scour depth for a single circular pile in steady currents for clear-water scour [52] and live-bed scour [15] conditions. The present test cases belong to live-bed scour; this is

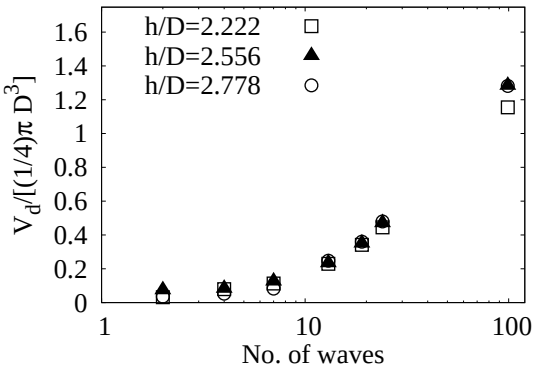

Fig. 18: The calculated total deposition volumes for three different water depth and a fixed wave height $H/D = 0.667$.

because the values of the Shields parameter for all test cases (see Table 1) are larger than the critical Shields parameter of about 0.06 according to Madsen and Grant [53].

For live-bed scour, the following empirical formula has been proposed by Sumer et al. [15] to estimate the dimensionless instantaneous scour depth $s(t_n)/D$ for a single pile,

$$\frac{s(t_n)}{D} = \left[1 - \exp\frac{-t_n}{t^*}\right]\frac{s_e}{D}, \tag{5}$$

where s_e is the equilibrium scour depth, t^* is a dimensionless characteristic time scale for the scour process and t_n is a dimensionless scour time. We stress that both t^* and t_n must use the same time scale to make them dimensionless. This formula has been applied to not only steady currents but also tidal currents [10] and oscillatory flows such as regular and irregular waves [9].

To use Eq. (5) to analyze the measured scour-hole depth, we can relate the number of solitary waves passed to a dimensionless equivalent scour time t_n by using the equivalent period T_s for a solitary wave defined in Eq. (1). The dimensionless equivalent scour time t_n after running n waves can be calculated by

$$t_n = nT_s/T_0, \tag{6}$$

where the time scale T_0 has been defined in Eq. (3). Both the dimensionless times t_* and t_n are normalized by T_0 in this section. Using Eq. (6) in Eq. (5), it is possible to fit Eq. (5) to the measured scour depths to obtain the values of s_e/D and t^* for the present problem. The fitting results are shown in Fig. 19 for all test cases, and the fitted values of s_e/D and t^* for all test cases are listed in Table 2. Note that for all test cases the bed profiles reach their near-equilibrium states after running 99 waves.

Table 2: Data fitting results for s_e/D and t^*.

Effects of Wave Height			Effects of Water Depth		
H/D	s_e/D	t^*	h/D	s_e/D	t^*
0.444	0.736	0.1438	2.222	0.984	0.0712
0.667	1.032	0.0905	2.556	1.004	0.0849
0.889	1.222	0.0750	2.778	1.032	0.0905

The good agreement between the measured and predicted evolution of the scour hole depths for all test cases, as shown in Fig. 19, implies the following two points:

1. Using Eq. (6) to convert the number of solitary waves into an equivalent time is appropriate.
2. Eq. (5), originally proposed for a single cylinder under steady currents or oscillatory flows, can be used to predict the evolution of the maximum depth of the scour hole at a row of closely-spaced cylinder under various solitary-wave conditions.

Sumer et al. [11] proposed an empirical formula for equilibrium scour depth s_e/D at a single vertical pile sitting in regular waves, which was later extended by Sumer and Fredsøe [54] and Ong et al. [26] to the following two conditions: (i) combined waves and current, and (ii) irregular waves. We attempted to fit these formulas to the results of s_e/D given in Table 2. After treating the coefficients related to flow conditions as the fitting parameters in the formula given in Sumer and Fredsøe [54], we obtained the following empirical formula for our data

$$\frac{s_e}{D} = 1.3\left[1 - e^{-0.7383(KC-5.6253)}\right], KC = \frac{U_m T_s}{D}, \tag{7}$$

which gives a moderately acceptable fit to our results with the maximum relative error being 22%. In Eq. (7), U_m is the peak horizontal velocity and the equivalent period T_s is defined by Eq. (1). The details can be found in Appendix C.

For the dimensionless time scale t^*, Sumer et al. [15] proposed Eq. (8) to calculate the value of t^* for given sediment characteristics and dimensions of the cylinder under steady current conditions.

$$t^* = \beta_1 \frac{h}{D}\left[\frac{u_*^2}{g(\gamma-1)d}\right]^{\beta_2}, \tag{8}$$

where γ is the specific gravity of the sediment, $u_* = \sqrt{\tau_b/\rho_w}$ is the shear velocity with τ_b being the bed shear stress, d is the mean sediment particle diameter, and β_1 and β_2 are two fitting parameters. Note that the term in the square brackets in Eq. (8) is basically the Shield parameter. For steady currents, Sumer et al. [15] suggested $\beta_1 = 1/2000$ and $\beta_2 = -2.2$.

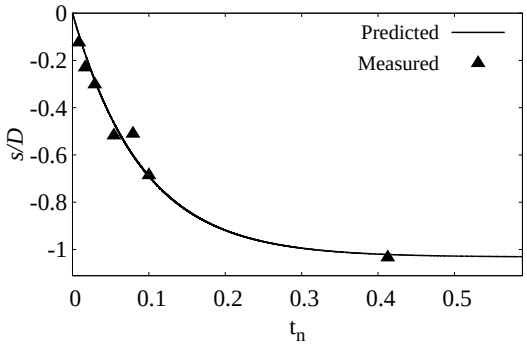

Case 1: $h/D = 2.778$ and $H/D = 0.667$

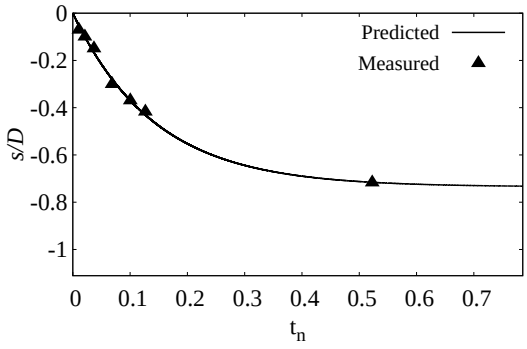

Case 2: $h/D = 2.778$ and $H/D = 0.444$

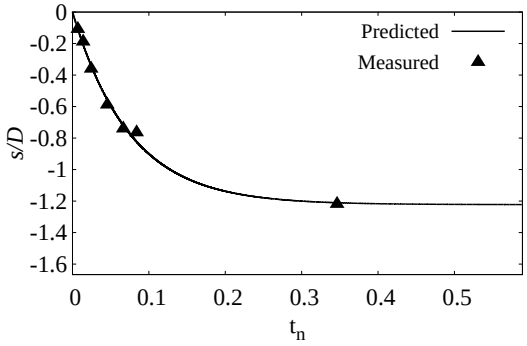

Case 3: $h/D = 2.778$ and $H/D = 0.889$

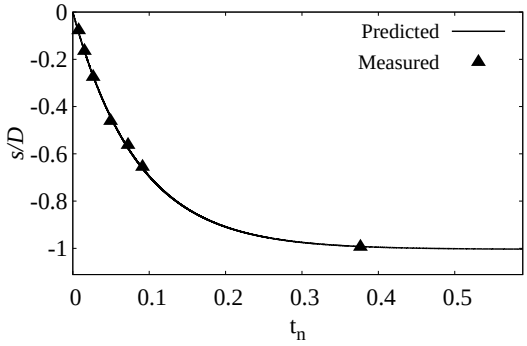

Case 4: $h/D = 2.556$ and $H/D = 0.667$

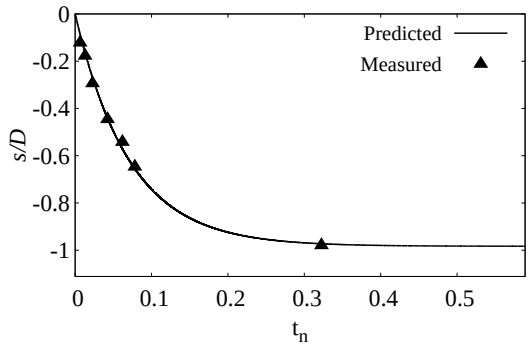

Case 5: $h/D = 2.222$ and $H/D = 0.667$

Fig. 19: Results obtained from fitting Eq. (5) to the measured scour-help depth for the five tested cases.

Sumer et al. [15] also proposed a formula for computing t^* for regular waves, which involves Keulegan-Carpenter (KC) number. Because the solitary wave is unidirectional, it seems reasonable to use the formula for steady currents; however, the parameters β_1 and β_2 obtained for steady currents may not be directly applicable to scour induced by solitary waves (see Appendix C for a discussion of using KC number to predict the equilibrium scour depth for solitary waves). The parameters β_1 and β_2 for the present test conditions should be obtained by fitting Eq. (8) to the data for

t^* given in Table 2.

To use Eq. (8) for solitary waves, we need to calculate the shear velocity u_* for a given solitary wave. Unlike for steady currents, shear velocity for a solitary wave varies with time. In anticipation that the sediment transport caused by solitary waves is controlled mainly by the maximum bottom shear stress, the theoretical solution of Liu et al. [55] for the bottom shear stress associated with a passing solitary wave (Fig. 2 in Liu et al. [55]) was used to calculate the maximum bed shear velocity u_* during a solitary wave. With u_* known, we fitted Eq. (8) to the data of t^* given in Table 2 to obtain an estimation of β_1 and β_2 in Eq. (8). The fitted values of β_1 and β_2 for the scour at a pile breakwater caused by solitary waves were found to be $\beta_1 = 0.0078$ and $\beta_2 = -0.9691$, i.e., the time scale t^* for the present tests is

$$t^* = \frac{0.0078h}{D}\left[\frac{u_*^2}{g(\gamma-1)d}\right]^{-0.9691} \tag{9}$$

The left panel of Fig. 20 shows a comparison between the measured and predicted t^* values using Eq. (9), and it can be seen that the agreement between the measured and predicted values of t_* is very good.

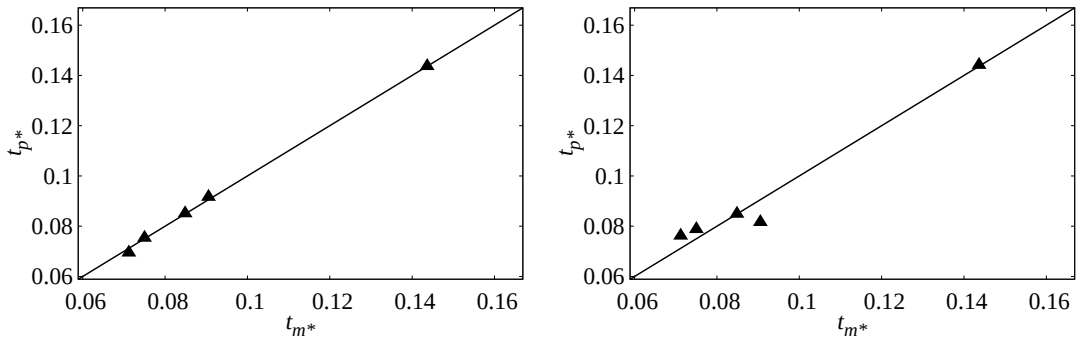

Fig. 20: A comparison of the measured and predicted values of the time scale t^*. The horizontal axis t_{m*} is the fitted value of t^* obtained from the measurement and the vertical axis t_{p*} is the predicted t^* using Eq. (9) or Eq. (10). Left panel is for from Eq. (9) and right panel is for Eq. (10) .

For solitary waves, $\beta_1 = 0.0078$, which is significantly larger than 1/2000, the value of β_1 for steady currents. This can be attributed to the use of the maximum bed shear velocity as the value of u_* in this analysis: the use of maximum bed shear velocity may overestimate the bed shear stress and hence require a larger value of β_1 to compensate the effect.

Using the KC number defined in Eq. (7), we can also use Eq. (10, which was proposed by Sumer et al. [15] for regular waves, to estimated t_*. Sumer et al. [15] proposed $\beta_3 = 10^{-6}$ and $\beta_4 = 3$ for regular waves and a single vertical pile. Fitting Eq. (10) to the values of t^* given in Table 2 gave $\beta_3 = 0.0028$ and $\beta_4 = 0.9738$ for the pile breakwater model and the solitary wave conditions tested in this study.

$$t^* = \beta_3\left(\frac{KC(\gamma-1)gd}{u_*^2}\right)^{\beta_4} \tag{10}$$

The right panel of Fig. 20 shows a comparison between the values of t^* predicted by Eq. (10) and the measured (i.e., those given in Table 2). It can be seen the values of t^* predicted by Eq. (10) agree reasonably well with the measured. Comparing the two plots in Fig. 20, it appears that Eq. (9) performs better than Eq. (10).

The good agreement between t_p^* and t_m^* as shown in Fig. 20 implies that Eq. (8), originally proposed for a single cylinder under steady currents and oscillatory flows, can also be applied to a row of closely-spaced cylinders under various solitary-wave conditions. However, it must be noted that the fitted values of β_1 and β_2 given in Eq. (9) are only valid for the tested pile breakwater configuration. It is expected that the values of these two fitting parameters depend on other factors such as the diameter of the piles, the gap size and sand diameter. Effects of these factors are worth further investigation.

Table 3: A summary of the characteristics of the final bed profile

Case	s/D	L_s/D	h_d/D	L_h/D	s_e/D	$V_s/[(1/4)\pi D^3]$	$V_d/[(1/4)\pi D^3]$
1	1.033	2.156	0.733	1.000	1.032	1.479	1.281
2	0.722	1.567	0.389	0.644	0.736	0.517	0.504
3	1.222	2.533	0.889	1.222	1.222	2.097	1.821
4	1.000	2.200	0.767	1.044	1.004	1.421	1.284
5	0.978	2.122	0.689	1.011	0.984	1.466	1.155

5. A summary of the characteristics of the final bed profile

Table 3 summarizes the key characteristics of the final bed profiles for the five test cases. The values of these characteristics are the values obtained after running 99 solitary waves. The equilibrium scour hole depth s_e/D, calculated using Eq. (5) through a data fitting, is also included for reference. These characteristics can be used for comparison with numerical simulations. One advantage of using solitary waves to verify and validate numerical models developed for studying scour at pile breakwaters is that it can avoid the computing time spent on establishing a steady state wave field in the presence of the multiple reflections of nonlinear periodic waves between the model and the wave generator.

6. Conclusions

In this study, the sediment scour around a pile breakwater (a row of closely spaced piles) under the action of multiple solitary waves was investigated experimentally. Using a high-resolution underwater laser scanner, in combination with a point probe, the temporal evolution of detailed three-dimensional bed profile near the pile breakwater was measured for three water depths and three wave heights. The following conclusions can be drawn from the experimental results reported in this study.

1. Scour occurred on both sides of the pile breakwater, and the maximum scour depth occurred in the gap between two piles. The maximum scour depth at the pile breakwater increased with increasing wave height. The maximum depth of the scour at the equilibrium state was found to be in the range of $0.73D$ and $1.22D$.
2. In the early stages of the scour process, the scour hole at the gap between two piles was shallow and not connected with the neighboring scour holes, the scour-depth contours had a U-shape pattern, and no sand bar on the down-wave side was observable. In the later stages of the scour process, the scour hole gradually joined with neighboring scour holes. When the scour profile approached its equilibrium state, a sand bar could form on the down-wave side of the scour hole. The sand bar height at its equilibrium state was found to be in the range of 0.35 D and 0.80 D.
3. For a fixed water depth, both the total scour volume and the deposition volume increased with increasing wave height. The total scour volume at equilibrium was found to be in the range of $0.52 \times[(1/4)\pi D^3]$ and $2.10 \times[(1/4)\pi D^3]$.
4. An existing formula, which was originally proposed for the evolution of the maximum depth of the scour at a single vertical cylinder under steady current or oscillatory flow conditions, was extended to a row of closely-spaced piles under solitary wave conditions. New empirical coefficients were obtained by fitting the formula to the new experimental data.
5. The maximum scour depth and the total scour volume were recommended as two reliable quantities for validation of numerical models developed for scour around pile breakwaters under highly nonlinear wave conditions.

The coefficients for the empirical formula describing the evolution of the scour hole depth are valid only for the test conditions examined in this study. The jet flow between two adjacent piles, which is affected by the gap size, is responsible for the local scour at the breakwater, and possible effects of gap size on the local scour at the pile breakwater is worth further investigation.

7. Acknowledgments

This work is supported by the US National Science Foundation under grant No. CBET-1706938. Any opinions, findings, and conclusions or recommendations expressed in this material are those of the author(s) and do not necessarily reflect the views of the National Science Foundation. The Hunan Province Key Laboratory of Water Sediment Sciences and Flood Hazard Prevention (China) is also acknowledged for its partial support to this work through grant No. 2017SS01. The authors would like to thank Dr. Jie Chen and Mr. Zengsheng Liu, both at the Changsha University of Science and Technology, and Mr. Peng Wang at the Zhejiang University, for their assistance during the experiment. This is SOEST contribution No. 11777.

Appendix A. A summary of existing experimental studies related to scour around vertical piles

In the past experimental studies of scour at vertical piles, four flow types have been examined on both standalone piles and groups of piles in the past. Table A.1 is a brief summary of structure types, flow types and key parameters found in the literature on experimental studies related to scour around vertical piles. The four flow types in Table A.1 are steady current (SC), tidal current (TC), regular wave (RW) and solitary wave (SW).

Table A.1: A summary of existing experimental studies related to scour around vertical piles.

Authors	Structure type	Flow type	Key parameters
Hayashi et al. [34]	Pile groups	RW	$T = 1.7$ s $h = 29.1$ cm $H = 2.68 - 9.37$ cm $D = 0.065$m; $d_{50} = 0.34 - 0.75$mm
Zhao et al. [4]	Submerged piles	SC	$h = 0.5$m; $D = 0.1$m; $d_{50} = 0.4$; $U = 0.362 - 0.441$m/s
Sumer and Fredsøe [33]	Pile groups	RW	$h = 0.4$m; $D = 0.032 - 0.09$m; $d_{50} = 0.2$mm; $T = 1.8 - 4.5$s; $KC = 3.0 - 37$
Sumer and Fredsøe [8]	Large standalone pile	RW	$h = 0.4$m; $D = 0.54 - 1.53$m; $d_{50} = 0.2$mm; $T = 2.0 - 3.5$s; $H = 2.5 - 12.0$cm; KC<1.4
Roulund et al. [5]	Standalone pile	SC	$h = 0.4$m; $D = 0.1$m; $d_{50} = 0.26$mm; $U = 0.46$m/s
McGovern et al. [10]	Standalone pile	SC/TC	$h = 0.1 - 0.4$m; $D = 0.2$m; $d_{50} = 0.135$mm; $U = 0.15 - 0.31$m/s; $T_{tide} = 54$min
Baykal et al. [9]	Standalone pile	SC/RW	$D = 0.04$m; $d_{50} = 0.17$mm; $h = 0.4$m; $U = 0.413$(Current); $T = 1.79 - 4.0$s
Amini et al. [7]	Pile group	SC	$h = 0.24$m; $D = 0.06$m; $d_{50} = 0.8$mm; $U = 0.3534 - 0.3645$
Sumer et al. [15]	Standalone circular pile	RW SC/TC	h=0.4m; D=0.01-0.2m; $d_{50} = 0.18 - 0.38$ mm; $T = 1.19 - 3.57$s; $KC = 4.9 - \inf$

Table A.1: A summary of existing experimental studies related to scour around vertical piles.

Authors	Structure type	Flow type	Key parameters
Escarameia and May [12]	Standalone pile	TC	$h = 0.0375-0.075$m; $d_{50} = 0.75$mm; $U = 0.239 - 0.430$m/s; D =various
Sheppard et al. [6]	Standalone large pile	SC	$h = 0.18 - 1.19$m; $D = 0.114 - 0.914$m; $d_{50} = 0.22 - 2.90$mm; $U = 0.29 - 0.76$m/s
Nakamura et al. [2]	Standalone large pile	SW	$h = 0.265 - 0.315$m; $D = 0.14$m; $H = 0.2-0.7$m; $d_{50} = 0.2-0.45$mm
Tonkin et al. [1]	Standalone pile	SW	$h = 2.45$m; $d_{50} = 0.35$mm; $D = 0.5$m; $H = 0.1 - 0.3$m
Chiew and Melville [56]	Standalone pile	SC	$h = 0.17$m; $D = 0.0318 - 0.045$m; $d_{50} = 0.24 - 3.2$mm
Lanca et al. [31]	Pile groups	SC	$U = 0.31$ m/s $h = 0.20$m; $D = 0.05$m; $d_{50} = 0.86$mm
Ataie-Ashtiani and Beheshti [28]	Pile groups	SC	$U = 0.21$ m/s $D = 0.016 - 0.028$m; $d_{50} = 0.25 - 0.98$mm
Amini and Solaimani [29]	Pile groups	SC	$U = 0.31$ m/s $D = 0.04$m; $d_{50} = 0.9$mm
Melville and Chiew [52]	Standalone pile	SC	$h = 0.02 - 0.2$m; $D = 0.016 - 0.2$m; $d_{50} = 0.90 - 5.35$mm; $U = 0.171 - 1.00$m/s

Even though scour at a group of piles has been studied experimentally in the past, all the existing experimental studies, with the exception of Hayashi et al. [34], focused on 3D configurations where the end effects may affect the measured scour profiles. A summary of the pile layouts in the existing studies involving more than two piles is given in Table A.2.

Table A.2: A summary of the pile layouts in the existing studies involving more than two piles.

No.	Authors	Model layout	Gap-diameter ratio	Comments
1	Zhao et al. [4]	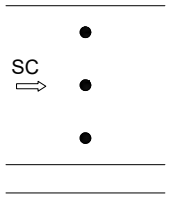	$n = 12.5$	Submerged
2	Sumer and Fredsøe [33]	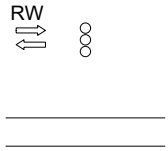	$n = 0.0 - 3.0$	Emergent
3	Amini et al. [7]	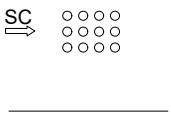	$n = 2.0 - 4.5$	Emergent
4	Ataie-Ashtiani and Beheshti [28]		$n = 0.0 - 6.0$	Emergent
5	Lanca et al. [31]		$n = 0.0 - 5.0$	Emergent
6	Amini and Solaimani [29]	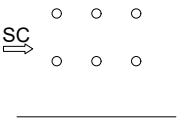	$n = 0.0 - 5.0$	Emergent
7	Hayashi et al. [34]	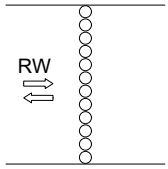	$n = 0.041 - 0.20$	Emergent
8	Present Study	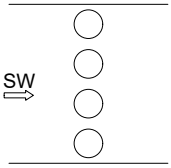	$n = 0.389$	Emergent

Appendix B. Repeatability and uncertainty

In order to evaluate the repeatability of and the uncertainty in the experimental results, repeating tests were conducted under the same test condition (H/D=0.889, h/D=0.278). An uncertainty analysis was conducted using the data collected for this set of repeating tests. After analyzing various possible sources of uncertainty, it was concluded that the major source of uncertainty came from the small differences in the initial bed profiles prepared for the repeating tests. When preparing the initial bed profiles for the repeating tests, small differences in the initial bed profiles was inevitably introduced; these small differences altered small-scale turbulence features, affected local sediment transport, and thus induced a difference in the scour patterns in the early stages of the scour process.

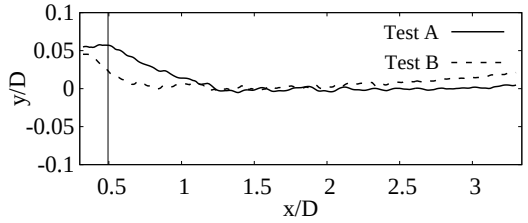

Fig. B.1: A comparison of the initial bed profiles along the transect A-A for the two repeating tests. The vertical line indicates the down-wave edge of the piles.

Fig. B.1 shows a comparison of the initial bed profiles along the transect A-A prepared for the two repeating tests (please refer to Fig. 8 in the main text for the definition of the transect A-A). For later discussion, we refer to these two repeating tests as Test A and Test B. Away from the model the initial profiles are relatively flat and agree reasonably well with each other; however, close to the model, especially inside the gap, the difference in the bed profiles prepared for the repeating tests is as large as 4.26 mm.

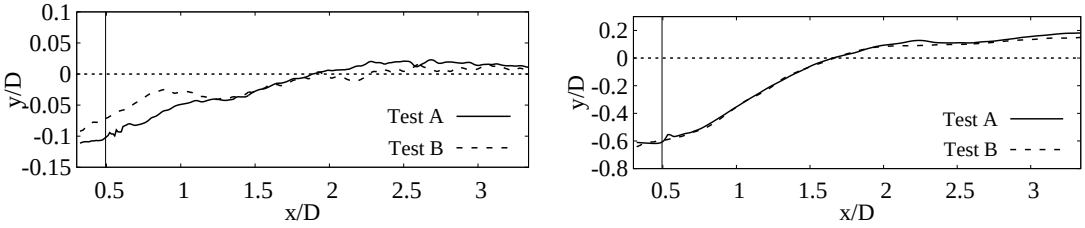

Fig. B.2: A comparison of the scour profiles along the transect A-A for the two repeating tests after four waves (left panel) and 19 waves (right panel). The vertical line indicates the edge of the piles.

Fig. B.2 shows a comparison of the measured scour profiles along the transect A-A for the two repeating tests after running four waves (left panel) and 19 waves (right panel). After running four waves, the difference between the two scour profiles is significant near the model, reaching as large as 3.74 mm in depth. The scour profile

shown in the left panel of Fig. B.2 is a good example of how minor change in local scour depth can significantly alter the measurement of the length of the scour hole L_s in the early stage of the scour process; therefore, the scour hole length is not a good quantity for numerical model validation in the early stage of the scour process. The results show that the difference in the measured scour depths for the repeating tests is small after running 19 waves. A comparison of scour profiles after 24 waves (not shown here) has shown similar agreement. It can be concluded that the uncertainty in the initial bed profile does not introduce noticeable uncertainty in the scour profile in the later stage of the scour process (say, after 19 waves for the present experiment).

Main results with error bars for the repeating tests ($h/D = 2.778$ and $H/D = 0.889$) are given in Fig. B.3.

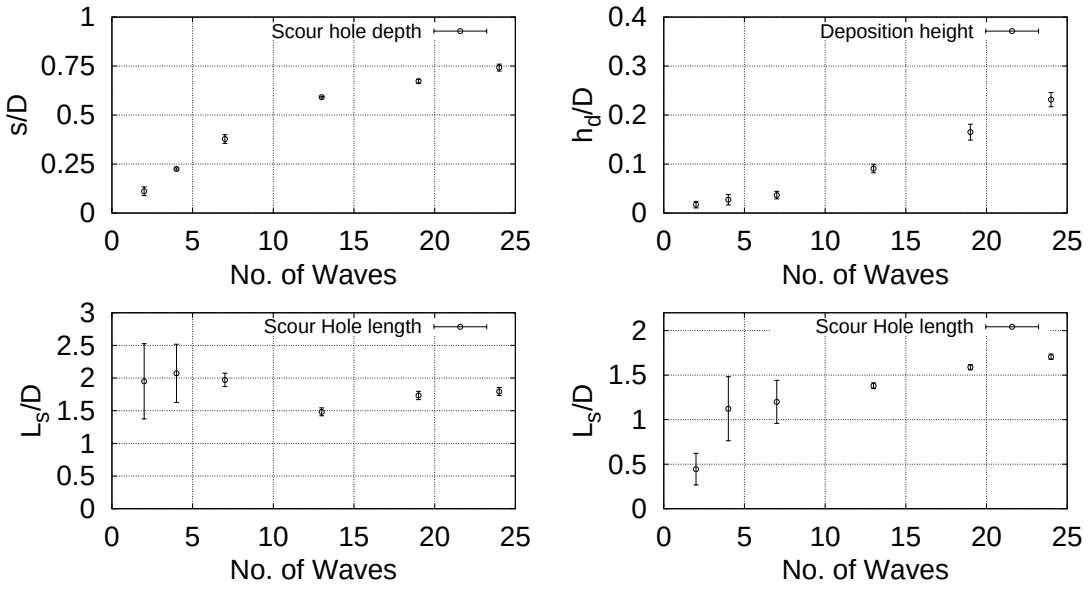

Fig. B.3: Error-bar plots of the scour hole depth s/D, deposition height h_d/D and scour hole length L_s/D of the repeatability tests. The bottom left panel is for the L_s/D determined based on zero-contour lines and the bottom right panel is for the L_s/D determined using -4 mm contour lines.

From Fig. B.3, it appears that the uncertainties in the maximum scour depth s/D and the maximum deposition height h_d/D are relatively small, in both the early stage and the later stage of the scour process. However, in the early stage, the measurement of scour hole length L_s may suffer large uncertainty when the zero-contour line is used (the same is true for L_h). We have also attempted to use -4-mm contour line to determine the scour hole length L_s/D, and the results are shown in the right panel of Fig. B.3. For both methods used to determine L_s, the error bars of L_s/D before 13 waves are large but small after 19 waves, indicating the overall uncertainty of L_s/D is very small in the later stage of the scour process. Therefore, for model validation purpose, only the results of L_s/D after 19 waves are included in this study.

Compared to the key scouring characteristic dimensions such as L_s and L_h, the uncertainties in the measured scour and deposition volumes are much smaller. A comparison of the measured scour and deposition volumes between Test A and Test B has shown that the maximum difference in these two repeating tests is less than 3% for the total scour volume and 5% for the total deposition volume.

Based on the analysis given above, we can conclude that the main difficulty in reducing the uncertainty in the measured L_s/D for the early stage of the scour process is because of the following reasons:

1. It is impossible to have exact same initial bed profile for repeating tests.
2. Small differences in the initial bed profile will affect the fine turbulence features which may affect local sediment transport.
3. L_s is defined by the zero-contour line, which has a very small slope in the early stages of the scour process. Therefore, in the early stages of the scour process, L_s can be greatly affected by a small difference in the initial bed profile.

Therefore, it is impossible to have an acceptable estimation of the error bar for L_s/D by repeating the test once or twice for each test condition.

Because the repeating tests have showed good repeatability and small measurement error and uncertainty in the scour-profile characteristics except for L_s/D and because repeating the test once or twice for each test condition cannot produce an acceptable estimation of the error bar for L_s/D, the experiment was designed to run each test condition once.

In view of the results presented above, it appears that the results of s/D, h_d/D, the total scour volume and the total deposition volume have good repeatability and low uncertainty even in the early stages, and the results of L_s/D have good repeatability and low uncertainty only after 13 waves. Therefore, the results of L_s/D for the early stages of the scour process (before 19 waves) should be excluded.

Appendix C. A discussion of the empirical formula of Sumer and Fredsøe [54] for equilibrium scour depth at a single vertical pile

In this appendix, three empirical formulas for the equilibrium scour depth at a single vertical pile are discussed. These formulas are all based on the work of Sumer et al. [11].

Sumer et al. [11] proposed the following formula for the prediction of the equilibrium scour depth s_e around a single vertical circular pile in waves:

$$\frac{s_e}{D} = 1.3\left[1 - e^{-0.03(KC-6)}\right], KC \geq 6.0, \tag{C1}$$

where D is the diameter of the circular pile and KC is the Keulegan-Carpenter number expressed by

$$KC = \frac{U_m T}{D}, \tag{C2}$$

with U_m being the maximum orbital flow velocity outside the wave bottom boundary layer and T the wave period. Later, Sumer and Fredsøe [54] extended the use of this formula to irregular waves and random waves plus a current. By inspecting the results using a number of combinations of statistical parameters, they found if the root mean square velocity U_{rms} and peak period T_p were used to compute KC number, Eq. (C1) could be applied to irregular waves as well. Sumer and Fredsøe [54] remarked that in the case of random wave plus a current, Eq. (C1) could be adapted to the following expression

$$\frac{s_e}{D} = c\left[1 - e^{a(KC-b)}\right], KC \geq b, \tag{C3}$$

where the coefficients a and b are given by:

$$a = -0.03 + 0.75U^{2.6}, \tag{C4}$$

$$b = 6e^{-4.7U}. \tag{C5}$$

In the expressions for a and b, the representative velocity is defined as $U = U_c/(U_c + U_{rms})$ with U_c being the current velocity outside the bottom boundary layer, and the coefficient c in Eq. (C3) represents the maximum possible dimensionless scour depth, for which Sumer et al. [11] suggested $c = 1.3$ (corresponding to the scenario of a steady current). Sumer et al. [21] also suggested the use of slightly larger values for c as a design safety measure. More recently, Ong et al. [26] proposed a stochastic method to predict the maximum equilibrium scour depth around a vertical pile under the influence of long-crested or short-crested random waves combined with currents. Based on Eq. (C3), Ong et al. [26] developed a sophisticated stochastic method for the determination of the expected value of s_e/D by considering the probability distribution of the incident waves and the effects of the largest $1/n$ waves.

Two major differences between regular/irregular waves and solitary waves are: (i) the lack of flow reversal in a solitary wave, and (ii) the lack of periodicity in a solitary wave. These differences require a new definition for KC number for solitary waves in order to use Eq. (C3) to estimate the equilibrium scour depth for the present experimental study. The reversal flow in regular/irregular waves can limit the maximum distance a water particle can travel in one direction. A solitary wave has a limited duration, which can also limit the maximum distance a water particle can travel in one direction. Therefore, if an equivalent period can be defined such that there are flow acceleration and deceleration within this equivalent period, it is possible to define a new KC number for solitary waves. Here we use the following equivalent wave period of a solitary wave for the wave period in Eq. (C2).

$$T_s = 4\pi\sqrt{\frac{h^3}{3gH(h+H)}}. \tag{C6}$$

For the characteristic velocity U_m in Eq. (C2), we use the maximum wave orbital velocity computed by using Grimshaw [49]'s solitary wave theory.

Table C.1: A summary of the calculation of equilibrium scour depth s_e/D using Eq. C1.

Case No.	$U_m[m/s]$	$T_s[s]$	KC	Measured s_e/D	s_e/D
1	0.343	2.12	8.084	1.032	0.079
2	0.240	2.69	7.170	0.736	0.045
3	0.428	1.78	8.461	1.222	0.093
4	0.354	1.94	7.624	1.004	0.062
5	0.383	1.66	7.064	0.984	0.041

Table C.1 shows the relevant parameters and the equilibrium scour depth predicted by using Eq. (C1). The s_e/D results as predicted by Eq. (C1) agree poorly with our experimental data: a significant under-prediction in equilibrium scour depth can be seen. This is partly because Eq. (C1) has been calibrated against a single vertical pile in a wave field. For an array of piles, the amplification of the bed shear stress due to the jet flow formed in between the piles is much stronger than the amplification of the bed shear stress due to the flow around a single vertical pile as tested by Sumer et al. [15].

Therefore, we attempted to use Eq. (C3) by obtaining a different set of coefficients using our present experimental data. We treated the value of coefficient c in Eq. (C3) as a constant of 1.3; this is because $s_e/D = 1.3$ is the equilibrium scour depth for steady currents and thus the limit for s_e/D as KC goes to infinity and because we believe the scours induced by solitary waves are not likely to exceed this limit. A nonlinear-least-square data fitting gave $a = -0.7383$ and $b = 5.6253$. Fig. C.1 shows a comparison between the prediction using Eq. (C3) and the measured equilibrium depth. The agreement between the predicted and measured equilibrium scour depths is only moderately acceptable, with a maximum difference of about 21.9%.

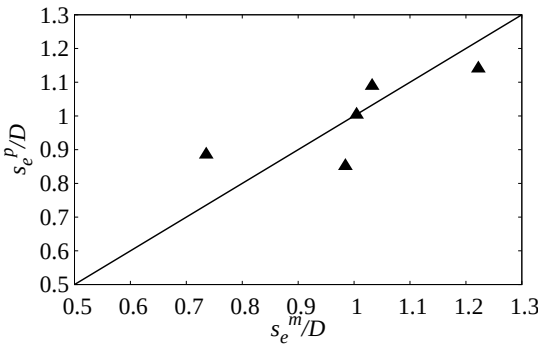

Fig. C.1: Comparison of the predicted equilibrium scour depth s_e^p using Eq. (C3) with coefficients obtained through data fitting and the measured equilibrium scour depth s_e^m.

References

[1] S. Tonkin, H. Yeh, F. Kato, S. Sato, Tsunami scour around a cylinder, Journal of Fluid Mechanics 496 (2003) 165–192.

[2] T. Nakamura, Y. Kuramitsu, N. Mizutani, Tsunami scour around a square structure, Coastal Engineering Journal 23101 (2) (2008) 209–246.

[3] J. Chen, Z. H. Huang, C. B. Jiang, B. Deng, Y. N. Long, Tsunami-induced scour at coastal roadways: A laboratory study, Natural Hazards 69 (1) (2013) 655–674.

[4] M. Zhao, L. Cheng, Z. Zang, Experimental and numerical investigation of local scour around a submerged vertical circular cylinder in steady currents, Coastal Engineering 57 (8) (2010) 709–721.

[5] A. Roulund, B. M. Sumer, J. Fredsøe, J. Michelsen, Numerical and experimental investigation of flow and scour around a circular pile, Journal of Fluid Mechanics 534 (2005) 351–401.

[6] D. M. Sheppard, M. Odeh, T. Glasser, Large scale clear-water local pier scour experiments, Journal of Hydraulic Engineering 130 (10) (2004) 957–963.

[7] A. Amini, B. W. Melville, T. M. Ali, A. H. Ghazali, Clear-water local scour around pile groups in shallow-water flow, Journal of Hydraulic Engineering 138 (2) (2012) 177–185.

[8] B. Sumer, J. Fredsøe, Wave scour around a large vertical circular cylinder, Journal of Waterway, Port, Coastal, and Ocean Engineering 127 (3) (2001) 125–134.

[9] C. Baykal, B. M. Sumer, D. R. Fuhrman, N. G. Jacobsen, J. Fredsøe, Numerical simulation of scour and backfilling processes around a circular pile in waves, Coastal Engineering 122 (February) (2017) 87–107.

[10] D. J. McGovern, S. Ilic, A. M. Folkard, S. J. McLelland, B. J. Murphy, Time development of scour around a cylinder in simulated tidal currents, Journal of Hydraulic Engineering 140 (6) (2014) 04014014.

[11] B. M. Sumer, J. Fredsøe, N. Christiansen, Scour around vertical pile in waves, Journal of waterway, port, coastal, and ocean engineering 118 (1) (1992) 15–31.

[12] M. Escarameia, R. W. P. May, Scour around structures in tidal flows, Tech. Rep. SR-522, HR Wallingford, Wallingford, 1999.

[13] M. Mattioli, J. M. Alsina, A. Mancinelli, M. Miozzi, M. Brocchini, Experimental investigation of the nearbed dynamics around a submarine pipeline laying on different types of seabed: the interaction between turbulent structures and particles, Advances in water resources 48 (2012) 31–46.

[14] C. Manes, M. Brocchini, Local scour around structures and the phenomenology of turbulence, Journal of Fluid Mechanics 779 (2015) 309–324.

[15] B. Sumer, N. Christiansen, J. Fredsøe, et al., Time scale of scour around a vertical pile, in: The Second International Offshore and Polar Engineering Conference, 3, International Society of Offshore and Polar Engineers, 308–315, 1992.

[16] A. J. Raudkivi, R. Ettema, Clear-water scour at cylindrical piers, Journal of Hydraulic Engineering 109 (3) (1983) 338–350.

[17] CEM, Coastal Engineering Manual, US Army Corps of Engineers, 2002.

[18] B. W. Melville, A. J. Raudkivi, Flow characteristics in local scour at bridge piers, Journal of Hydraulic Research 15 (4) (1977) 373–380.

[19] F. Ahmed, N. Rajaratnam, Flow around bridge piers, Journal of Hydraulic Engineering 124 (3) (1998) 288–300.

[20] A. Qadar, The vortex scour mechanism at bridge piers, in: Institution of Civil Engineers, Proceedings, Pt2, vol. 71, 1981.

[21] B. M. Sumer, et al., The mechanics of scour in the marine environment, vol. 17, World Scientific Publishing Company, 2002.

[22] M. Muzzammil, T. Gangadhariah, The mean characteristics of horseshoe vortex at a cylindrical pier, Journal of Hydraulic Research 41 (3) (2003) 285–297.

[23] J. Unger, W. H. Hager, Down-flow and horseshoe vortex characteristics of sediment embedded bridge piers, Experiments in Fluids 42 (1) (2007) 1–19.

[24] G. Kirkil, S. Constantinescu, R. Ettema, Coherent structures in the flow field around a circular cylinder with scour hole, Journal of Hydraulic Engineering 134 (5) (2008) 572–587.

[25] H. Breusers, G. Nicollet, H. Shen, Local scour around cylindrical piers, Journal of Hydraulic Research 15 (3) (1977) 211–252.

[26] M. C. Ong, D. Myrhaug, P. Hesten, Scour around vertical piles due to long-crested and short-crested nonlinear random waves plus a current, Coastal Engineering 73 (2013) 106–114.

[27] B. M. Sumer, J. Fredsøe, Wave scour around structures, in: Advances in coastal and ocean engineering, World Scientific, 191–249, 1999.

[28] B. Ataie-Ashtiani, A. Beheshti, Experimental investigation of clear-water local scour at pile groups, Journal of Hydraulic Engineering 132 (10) (2006) 1100–1104.

[29] A. Amini, N. Solaimani, The effects of uniform and nonuniform pile spacing variations on local scour at pile groups, Marine Georesources & Geotechnology 0618 (November) (2017) 1–6.

[30] A. Amini, B. W. Melville, T. M. Ali, A. H. Ghazali, Clear-water local scour around pile groups in shallow-water flow, Journal of Hydraulic Engineering 138 (2) (2011) 177–185.

[31] R. Lanca, C. Fael, R. Maia, J. P. Pego, A. H. Cardoso, Clear-water scour at pile groups, Journal of Hydraulic Engineering 139 (10) (2013) 1089–1098.

[32] M. Zdravkovich, The effects of interference between circular cylinders in cross flow, Journal of fluids and structures 1 (2) (1987) 239–261.

[33] B. Sumer, J. Fredsøe, Wave scour around group of vertical piles, Journal of Waterway, Port, Coastal, and Ocean Engineering 124 (5) (1998) 248–256.

[34] T. Hayashi, M. Hattori, M. Shirai, Closely spaced pile breakwater as a protection structure against beach erosion, in: Coastal Engineering 1968, 606–621, 1969.

[35] P. A. Madsen, D. R. Fuhrman, H. A. Schäffer, On the solitary wave paradigm for tsunamis, Journal of Geophysical Research: Oceans 113 (C12012) (2008) 1–22.

[36] B. M. Sumer, M. B. Sen, I. Karagali, B. Ceren, J. Fredsøe, M. Sottile, L. Zilioli, D. R. Fuhrman, Flow and sediment transport induced by a plunging solitary wave, Journal of Geophysical Research: Oceans 116 (1) (2011) 1–15.

[37] S. Kakuno, P. L. F. Liu, Scattering of water waves by vertical cylinders, Journal of Waterway,Port,Coastal,and Ocean Engineering 119 (3) (1993) 302–322.

[38] K. D. Suh, C. H. Ji, B. H. Kim, Closed-form solutions for wave reflection and transmission by vertical slotted barrier, Coastal Engineering 58 (12) (2011) 1089–1096.

[39] Z. H. Huang, Y. C. Li, Y. Liu, Hydraulic performance and wave loadings of perforated/slotted coastal structures:A review, Ocean Engineering 38 (2011) 1031–1053.

[40] H. Yeh, P. Liu, M. Briggs, C. Synolakis, Propagation and amplification of tsunamis at coastal boundaries, Nature 372 (6504) (1994) 353.

[41] M. J. Briggs, C. E. Synolakis, G. S. Harkins, D. R. Green, Laboratory experiments of tsunami runup on a circular island, Pure and applied geophysics 144 (3-4) (1995) 569–593.

[42] P. L.-F. Liu, Y.-S. Cho, M. J. Briggs, U. Kanoglu, C. E. Synolakis, Runup of solitary waves on a circular island, Journal of Fluid Mechanics 302 (1995) 259–285.

[43] J. Chen, Z. Huang, C. Jiang, B. Deng, Y. Long, An experimental study of changes of beach profile and mean grain size caused by tsunami-like waves, Journal of Coastal Research 28 (5) (2012) 1303–1312.

[44] Y. L. Young, H. Xiao, T. Maddux, Hydro- and morpho-dynamic modeling of breaking solitary waves over a fine sand beach. Part I: Experimental study, Marine Geology 269 (3-4) (2010) 107–118.

[45] T. Rossetto, W. Allsop, I. Charvet, D. I. Robinson, Physical modelling of tsunami using a new pneumatic wave generator, Coastal Engineering 58 (6) (2011) 517–527.

[46] S. Shafiei, B. W. Melville, A. Y. Shamseldin, Experimental investigation of tsunami bore impact force and pressure on a square prism, Coastal Engineering 110 (2016) 1–16.

[47] D. Goring, F. Raichlen, The generation of long waves in the laboratory, in: Seventeenth International Conference on Coastal Engineering Conference, vol. 1, American Society of Civil Engineers, 763–783, 1980.

[48] Z. H. Huang, Z. D. Yuan, Transmission of solitary waves through slotted barriers: A laboratory study with analysis by a long wave approximation, Journal of Hydro-Environment Research 3 (4) (2010) 179–185.

[49] R. Grimshaw, The solitary wave in water of variable depth. Part 2, Journal of Fluid Mechanics 42 (03) (1971) 639–656.

[50] W. Li, H. Yeh, Y. Kodama, On the Mach reflection of a solitary wave: revisited, Journal of Fluid Mechanics 672 (2011) 1–32.

[51] R. Soulsby, Dynamics of marine sands: a manual for practical applications, Thomas Telford, 1997.

[52] B. W. Melville, Y. M. Chiew, Time scale for local scour at bridge piers, Journal of Hydraulic Engineering 125 (1) (1999) 59–65.

[53] O. S. Madsen, W. D. Grant, Quantitative description of sediment transport by waves, in: Fifteenth International Conference on Coastal Engineering, vol. 2, American Society of Civil Engineers, 1093–1112, 1976.

[54] B. M. Sumer, J. Fredsøe, Scour around pile in combined waves and current, Journal of Hydraulic Engineering 127 (5) (2001) 403–411.

[55] P. L. F. Liu, Y. S. Park, E. A. Cowen, Boundary layer flow and bed shear stress under a solitary wave, Journal of Fluid Mechanics 574 (2007) 449–463.

[56] Y. Chiew, B. Melville, Local scour around bridge piers, Journal of Hydraulic Research 25 (1) (1987) 15–26.